8-2010

A Diagnostic Examination of Consecutive Extreme Cool-Season Precipitation Events at St. John's, Newfoundland, in December 2008

Shawn M. Milrad
McGill University, milrads@erau.edu

Eyad H. Atallah
McGill University

John R. Gyakum
McGill University

Scholarly Commons Citation

Milrad, S. M., Atallah, E. H., & Gyakum, J. R. (2010). A Diagnostic Examination of Consecutive Extreme Cool-Season Precipitation Events at St. John's, Newfoundland, in December 2008. *Weather and Forecasting, 25*(4). https://doi.org/10.1175/2010WAF2222371.1

A Diagnostic Examination of Consecutive Extreme Cool-Season Precipitation Events at St. John's, Newfoundland, in December 2008

SHAWN M. MILRAD, EYAD H. ATALLAH, AND JOHN R. GYAKUM

Department of Atmospheric and Oceanic Sciences, McGill University, Montreal, Quebec, Canada

(Manuscript received 23 October 2009, in final form 17 March 2010)

ABSTRACT

St. John's, Newfoundland, Canada (CYYT), is frequently affected by extreme precipitation events, particularly in the cool season (October–April). Previous work classified precipitation events at CYYT into categories by precipitation amount and a manual synoptic typing was performed on the 50 median extreme precipitation events, using two separate methods. Here, consecutive extreme precipitation events in December 2008 are analyzed. These events occurred over a 6-day period and produced over 125 mm of precipitation at CYYT. The first manual typing method, using a backward-trajectory analysis, results in both events being classified as ''southwest,'' which were previously defined as the majority of the backward trajectories originating in the Gulf of Mexico. The second method of manual synoptic typing finds that the first event is classified as a ''cyclone,'' while the second is a ''frontal'' event. A synoptic analysis of both events is conducted, highlighting important dynamic and thermodynamic structures. The first event was characterized by strong quasigeostrophic forcing for ascent in a weakly stable atmosphere in association with a rapidly intensifying extratropical cyclone off the coast of North America and transient high values of subtropical moisture. The second event was characterized by primarily frontogenetical forcing for ascent in a weakly stable atmosphere in the presence of quasi-stationary high values of subtropical moisture, in association with a northeast–southwest-oriented baroclinic zone situated near CYYT. In sum, the synoptic structures responsible for the two events highlight rather disparate means to produce an extreme precipitation event at CYYT.

1. Introduction

Atlantic Canada (Fig. 1), and more specifically, St. John's, Newfoundland (CYYT), is a location susceptible to extreme precipitation events, particularly in the cool season (Stewart et al. 1987), defined in Milrad et al. (2009) as October–April. Located at the confluence of several North American storm tracks (Milrad et al. 2009) and near the convergence zone of the cold southward-flowing Labrador Current and the warm northward-flowing Gulf Stream current (Aguado and Burt 2007, p. 227), CYYT is prone to extreme precipitation events, often associated with intense cyclogenesis.

In Milrad et al. (2009), categorical amounts of precipitation (e.g., extreme, moderate, and light) were defined for cool-season precipitation events at CYYT from 1979 to 2005. Subsequently, statistically significant composite synoptic-scale structures and precursors were identified up to 72 h before the onset of the heaviest precipitation at CYYT.

Milrad et al. (2010) detailed the manual synoptic typing of the 50 extreme events defined in Milrad et al. (2009). This was accomplished by two separate partitioning methods. The first method utilized a 5-day backward-trajectory analysis, which separated extreme precipitation events by air parcel source region. Three types of events were established: south, southwest, and west. South events were generally associated with relatively weak sea level cyclones that originated in the Atlantic Ocean south of CYYT and a strong sea level anticyclone downstream of CYYT. Southwest events were those with air parcels originating in the Gulf of Mexico and were typically caused by an intense sea level cyclone that formed in the Gulf of Mexico and rapidly intensified as it moved northeast toward CYYT. West events were associated with sea level cyclones that took an Alberta Clipper track and contained strong upper-tropospheric

Corresponding author address: Shawn M. Milrad, Dept. of Atmospheric and Oceanic Sciences, McGill University, 805 Sherbrooke St. W., Montreal QC H3A 2K6, Canada.
E-mail: shawn.milrad@gmail.com

DOI: 10.1175/2010WAF2222371.1

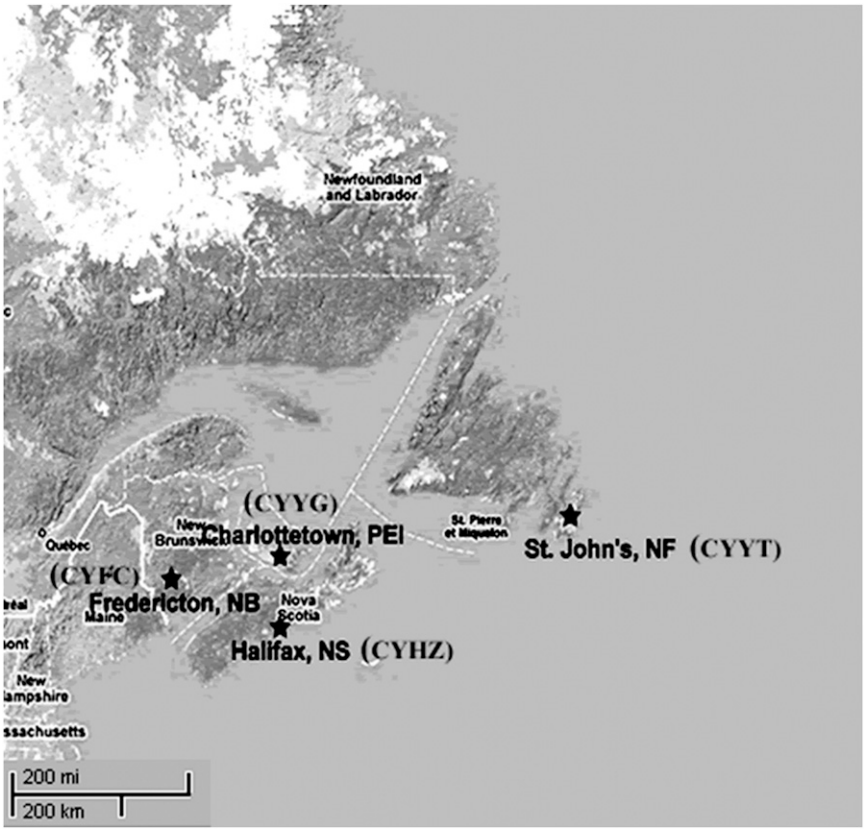

FIG. 1. The geography of Atlantic Canada, with the capital city of each province identified, and scale as shown.

dynamics that did not produce a strong sea level cyclone until reaching less stable air over the Atlantic Ocean.

The second partitioning method in Milrad et al. (2010) revolved around three commonly used quasigeostrophic (QG) ascent-forcing variables: low-tropospheric horizontal temperature advection, midtropospheric vorticity advection, and low-tropospheric frontogenesis. Two event types were established—cyclone and frontal. The composite features in the cyclone group exhibited a strong sea level cyclone originating in the Gulf of Mexico. In contrast, the frontal group composite displayed a relatively benign synoptic pattern dominated by a downstream anticyclone, strong southerly flow and moisture transport into CYYT, and a northeast–southwest-oriented baroclinic zone that was quasi-stationary near CYYT.

The goal of this study is to apply the lessons learned and synoptic types of Milrad et al. (2010) to an investigation of consecutive extreme precipitation events at CYYT in December 2008. These events occurred from 7 to 12 December 2008. During this time, over 125 mm of precipitation was recorded at CYYT. The precipitation totals for each event rank in the top 20 cool-season precipitation events at CYYT since 1979 (Milrad et al. 2009). The first event (hereafter MAG 1), from 1200 UTC 7 December to 1200 UTC 9 December, resulted in 73.6 mm of precipitation, while the second event (hereafter MAG 2), from 0000 UTC 11 December to 0000 UTC 13 December, resulted in 54 mm of precipitation.

Case studies of extreme precipitation events (often involving intense cyclogenesis) are not new in atmospheric science. The Presidents' Day snowstorm of 18–19 February 1979 was outlined by Bosart (1981), Bosart and Lin (1984), Uccellini et al. (1984, 1985), and Whitaker et al. (1988). Bosart (1981) found that the rapid deepening of the sea level cyclone could not fully be explained using quasigeostrophic theory and was also related to convection near the storm center. Bosart and Lin (1984) argued that a tropopause fold was present west of the cyclone, in addition to the presence of in situ low-level vorticity near the center of the evolving sea level cyclone. Uccellini et al. (1984) isolated three separate jet streaks that played a crucial role in the evolution of the storm, especially during the period of rapid cyclogenesis, while Uccellini et al. (1985) closely examined the tropopause fold and extrusion of stratospheric air associated with an intensifying upper-level trough

located to the west of the sea level cyclone. Finally, Whitaker et al. (1988) utilized a backward-trajectory analysis to identify different airstreams that converge into the region of cyclogenesis.

Kocin et al. (1995) discussed the storm track, precipitation amounts, and damage caused by the Superstorm of 12–14 March 1993. Time series of satellite imagery were provided and showed the classic comma-cloud structure expected from a rapidly intensifying cool-season cyclone. Moreover, Bosart et al. (1996) and Dickinson et al. (1997) presented an analysis of the upper-tropospheric dynamics of the Superstorm using potential vorticity (PV) analyses on the dynamic tropopause (DT), the latter of which included a discussion of the enhancement of the downstream upper-level ridge due to latent heat release from extreme precipitation. Dickinson et al. (1997) also commented on the fact that the Gulf of Mexico is a well-known source region for cyclogenesis, albeit one in which rapid intensification is rarely seen. Finally, Huo et al. (1995) focused on the static stability of the environment prior to and during rapid cyclogenesis and the interaction of positive PV anomalies on the DT.

Other important events in the past 30 years include but are not limited to the ''surprise'' snowstorm over the mid-Atlantic region in January 2000 (Brennan and Lackmann 2006); the *Queen Elizabeth II* (*QE II*) cyclone of September 1978 (Uccellini 1986; Gyakum 1991); an explosive cyclogenesis event detailed by Wash et al. (1990), which was observed during the Genesis of Atlantic Lows Experiment (GALE); and the crippling ice storm of January 1998 (Gyakum and Roebber 2001; Roebber and Gyakum 2003).

The analyses of historical cases of extreme precipitation are important to this study because they serve as a basis for the synoptic analysis presented. Additionally, several points important to the cases in this study were highlighted, particularly in the case of MAG 1, which was associated with a rapidly intensifying sea level cyclone off the coast of North America.

Another motivation for this paper is the relative lack of literature regarding extreme precipitation events in Atlantic Canada. Much of the work on extreme precipitation events in Atlantic Canada was associated with occurrences of intense cyclogenesis during the Canadian Atlantic Storms Program (CASP) field project, phase I of which was conducted from January to March 1986 (Stewart et al. 1987), coinciding with GALE (Dirks et al. 1988), and phase II of which took place during the same period in 1992 (Stewart 1991). While much of the work associated with CASP I and II focused on mesoscale structures within East Coast cyclones (e.g., Stewart et al. 1990; Reuter and Yau 1990), a few published works detailed mechanisms for cases of intense cyclogenesis (e.g., Yau and Jean 1989; Stewart and Donaldson 1989; Gyakum et al. 1996; Gyakum and Stewart 1996; Huo et al. 1996). Gyakum et al. (1996) addressed the climatological characteristics of storm tracks and areas of cyclogenesis in the Atlantic Canada region. Gyakum et al. (1996) stated that while explosive intensification typically takes place off the east coast of the United States and Canada, the ''formative stages of these dangerous storms do occur in regions far upstream,'' and that proper analysis of these upstream features is crucial to producing an accurate forecast for Atlantic Canada.

2. Data and methods used

a. Data

This study utilizes 6-hourly precipitation data for CYYT, obtained from the Environment Canada 6-h corrected precipitation database. The corrected precipitation data are based on work done by Mekis and Hogg (1999), whereby the data were adjusted to accurately reflect precipitation gauge changes, wind conditions, and changes in station location. All precipitation data in this study were observed in liquid equivalent form (i.e., no data were acquired using ruler methods), limiting errors associated with frozen precipitation.

The National Centers for Environmental Prediction (NCEP) Global Forecast System (GFS) analysis, with a horizontal resolution of ½°, is used as the dataset for most synoptic analyses, which differs from the choice of analyses in Milrad et al. (2009, 2010), where the NCEP–NCAR Global Reanalysis with a horizontal resolution of 2.5° (Kalnay et al. 1996), and NCEP North American Regional Reanalysis (NARR; Mesinger et al. 2006), with a horizontal resolution of 32 km, were used. The authors believe that while the dataset does not extend far enough back historically to be used for the composites in Milrad et al. (2009, 2010), the GFS ½° analysis is a superior tool for MAG 1 and 2, primarily in terms of resolution compared to the NCEP–NCAR Global Reanalysis, and accuracy compared to the NARR; the latter of these concerns revolves around the precipitation assimilation scheme over Canada in the NARR (M. Carrera 2008, personal communication), which will be further detailed in the future. However, the authors note that the NCEP–NCAR Global Reanalysis is used here for diagnostics of **Q**-vector divergence and for gridpoint diagnostics of the QG-forcing parameters defined in Milrad et al. (2010). This is done for two reasons: 1) to be consistent with the QG-forcing synoptic-typing methodology of Milrad et al. 2010, which used the NCEP–NCAR Global Reanalysis, and 2) while the authors believe the GFS ½° analysis is generally a superior tool to the NCEP–NCAR Global Reanalysis for dynamic and thermodynamic diagnostics,

errors were found in relatively noisy fields (e.g., **Q**-vector divergence) and point calculations using the higher-resolution analysis. For the sake of completeness, it has been found that the large-scale dynamics and thermodynamics shown in this paper display qualitatively similar results in both analysis tools (not shown). These points are discussed further in sections 3a and 4a.

The backward-trajectory analysis is performed using the National Oceanic and Atmospheric Administration/Air Resources Laboratory's (NOAA/ARL) Hybrid Single Particle Lagrangian Integrated Trajectory Model (HYSPLIT; information available online at http://www.arl.noaa.gov/HYSPLIT.php). The radar data were provided by Environment Canada's Atlantic Climate Centre and the satellite imagery was obtained from NOAA's Comprehensive Large Array Data Stewardship System (CLASS; available online at http://www.class.ncdc.noaa.gov/saa/products/welcome). The vast majority of the calculations and analyses in this study are displayed using the General Meteorological Package (GEMPAK), version 5.11.1 [updated from the original package devised by Koch et al. (1983)], a data manipulation and visualization software package.

b. Methods used

The methods used in this study revolve around two main points:

- The application of both methods of manual synoptic typing outlined in Milrad et al. (2010) to MAG 1 and MAG 2, as well as a validation of the composite synoptic structures observed for the median extreme cases (Milrad et al. 2009) and the various synoptic types (Milrad et al. 2010).
- The dynamic and thermodynamic analyses in sections 3b and 4b for MAG 1 and MAG 2, respectively, strive to illustrate the relative contributions of dynamic forcing and the thermodynamic properties of the air mass involved, to the heavy precipitation recorded in both events. Equation (1) relates the precipitation rate to the integrated ascent (assumed for the purpose of this paper to be quasigeostrophic) and incipient air mass, where precipitation (P) is assumed equal to condensation, g is the acceleration due to gravity, ω is the vertical motion in pressure coordinates, and $(dr_s/dp)_{\rm ma}$ is the saturation mixing ratio lapse rate along the moist adiabat. This equation was first published by Gyakum (2008), who states that "the transports of tropical air mass characteristics are crucial to the production of heavy precipitation in the extratropical latitudes." In addition, using the lapse rate along the moist adiabat as a measure of effective static stability, as presented in Eq. (1), suggests that weaker static stability, often associated with moist subtropical air masses, implies higher values of precipitation rate for a given value of ascent (Gyakum 2008):

$$P = -\frac{1}{g}\int \omega\left(\frac{dr_s}{dp}\right)_{\rm ma} dp. \qquad (1)$$

The definition of time $t = 0$ h is consistent with that established in Milrad et al. (2009, 2010) and refers to the onset of the 6-h period of maximum recorded precipitation at CYYT. Comparisons of backward trajectories and synoptic structures to the NCEP–NCAR Global Reanalysis and NARR have been made (not shown) and were confirmed to be similar.

3. MAG 1: 8 December 2008

a. Overview and synoptic typing

MAG 1 affected CYYT from 1200 UTC 7 December 2008 until 1200 UTC 9 December 2008, where $t = 0$ h is 0600 UTC 8 December 2008. Overall, 73.6 mm of precipitation fell at CYYT during MAG 1 (Fig. 2), which ranks as the fifth most extreme cool-season precipitation event since 1979 (Milrad et al. 2009). MAG 1 exceeded the median extreme event defined in Milrad et al. (2009) by approximately 30 mm. As shown in Fig. 2, most of the precipitation (63 mm) fell in a 24-h period from 1200 UTC 7 December to 1200 UTC 8 December. During this time period, the boundary layer at CYYT was almost completely saturated (Figs. 2a and 2b) and the temperature slowly rose from around 0°C at 1200 UTC 7 December to just above 10°C shortly after 0600 UTC 8 December. Subsequently, the surface proceeded to slowly cool, reaching a temperature of around −3°C by 1200 UTC 9 December, at the end of the event. Observed surface winds during MAG 1 shifted from easterly at 1200 UTC 7 December to southerly during the period of heaviest precipitation, from 0000 UTC 8 December to 1400 UTC 8 December and, finally, to westerly from 1400 UTC 8 December until the end of the event (Fig. 2). Light to moderate snow fell for the first few hours of the event (Fig. 2a) but quickly changed to light to moderate rain by 1700 UTC 7 December (Fig. 2a) and tapered to rain showers by 0000 UTC 9 December (Fig. 2c) and, finally, light snow by 1000 UTC 9 December (Fig. 2c). The observations of temperature trends, wind shifts, and precipitation types are consistent with the passage of a typical midlatitude cyclone at CYYT. Moreover, the wind shift to the south just before 0000 UTC 8 December (Fig. 2a) is consistent with a spike in surface temperature associated with a warm front that moved through

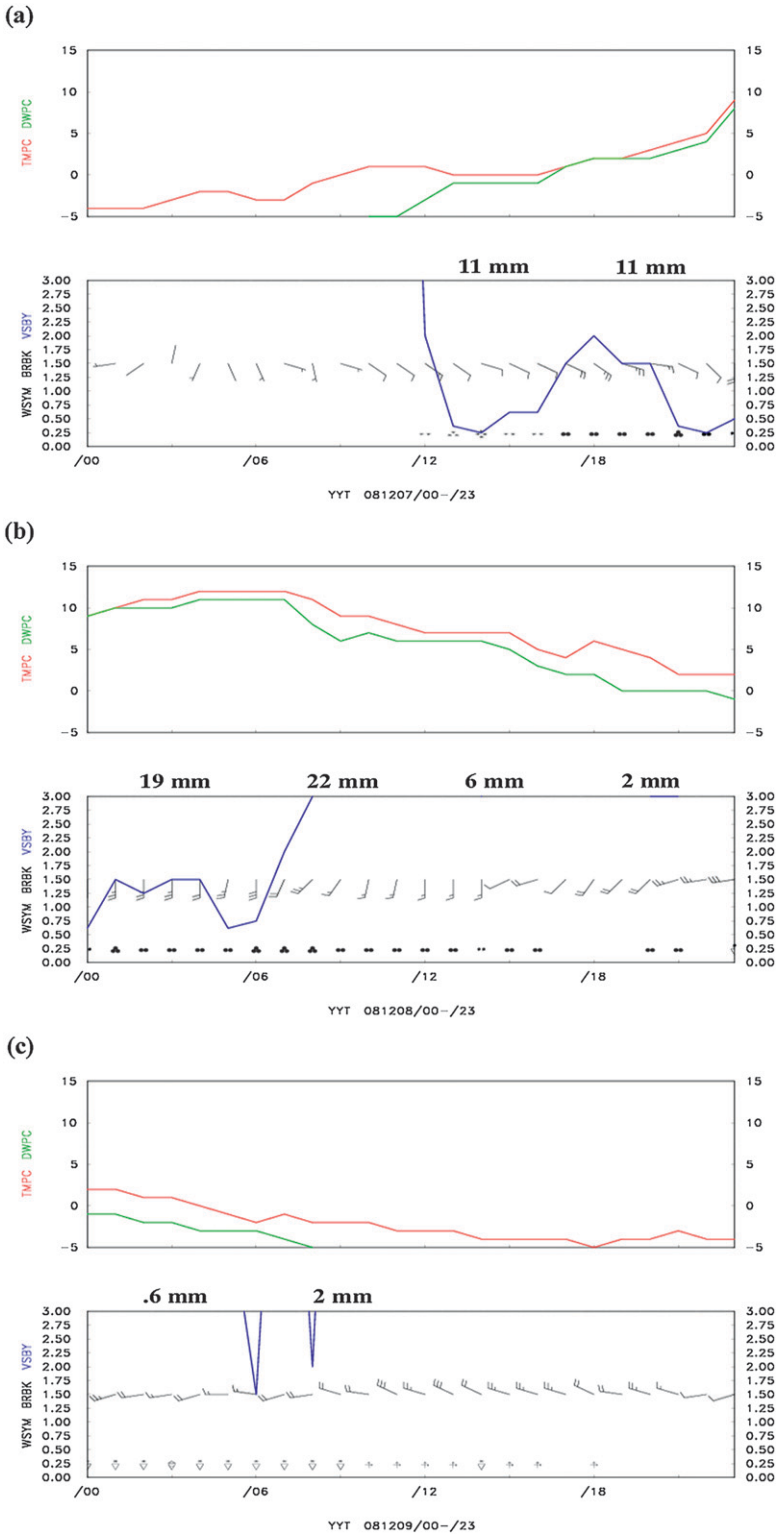

FIG. 2. Meteograms for the entire period of precipitation at CYYT for MAG 1. In the top panels of (a) 7, (b) 8, and (c) 9 Dec 2008, temperatures (dewpoints) are plotted in red (green), and are in °C. In the bottom panel of (a)–(c), time on the horizontal axis is in UTC, visibility (statute miles) on the vertical axis is plotted in blue (not shown for values >3 statute miles), wind (kt) is represented by barbs, and 6-h precipitation amounts are set in boldface.

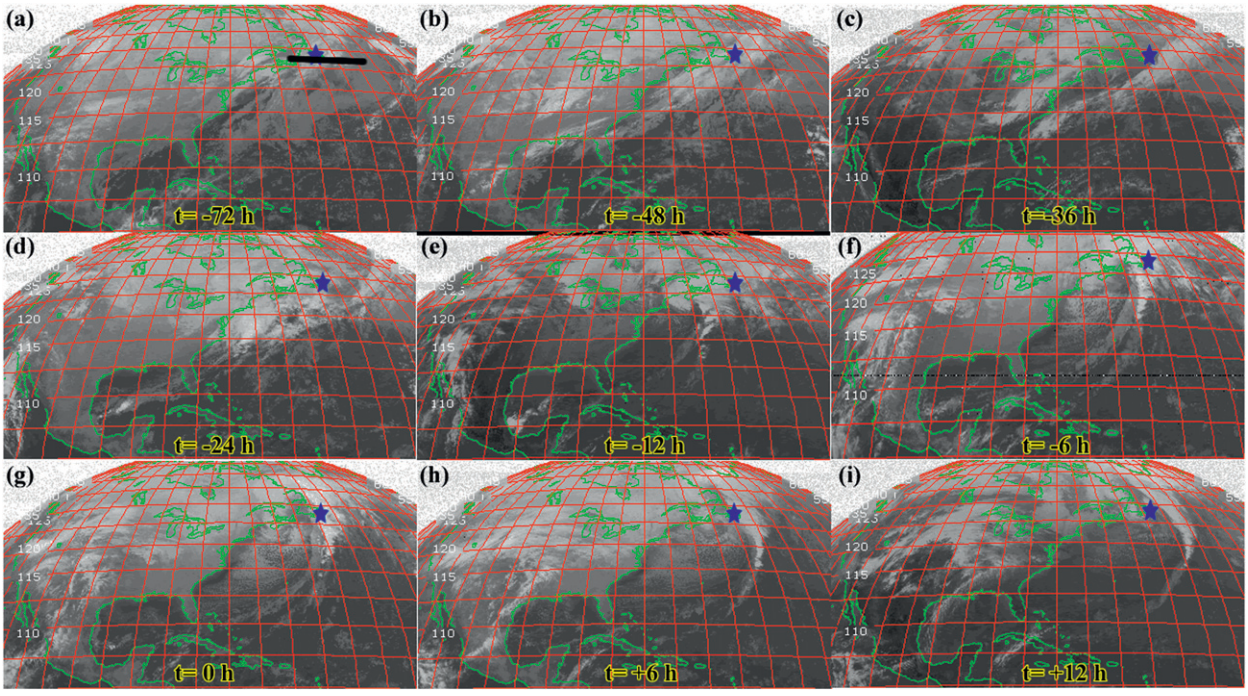

FIG. 3. Time series of infrared satellite imagery for MAG 1. Images are presented for t = (a) −72, (b) −48, (c) −36, (d) −24, (e) −12, (f) −6, (g) 0, (h) +6, and (i) +12 h, where t = 0 h is 0600 UTC 8 Dec 2008. A blue star is placed in each panel at the approximate location of CYYT and the area of interest explored in Fig. 11 (cross section) is outlined with a black line in (a).

CYYT in advance of the sea level cyclone. The subsequent wind shift to the west after 1800 UTC 8 December (Fig. 2b) and the accompanying surface temperature drop were associated with the passage of a trailing cold front. The heaviest precipitation at CYYT during MAG 1 occurred when the station was located in the warm sector of the cyclone, while the surface winds were onshore (southerly). Finally, the observation of easterly surface winds during part of MAG 1 is consistent with the extreme composite in Milrad et al. (2009).

The evolution of MAG 1 is displayed in infrared satellite imagery in Fig. 3. A coastal cyclone was not evident until $t = -24$ h (0600 UTC 7 December), when an area of clouds was present off the coast of Virginia and North Carolina (Fig. 3d). By $t = -12$ h, the cyclone had acquired the typical comma-cloud structure often seen in intensifying extratropical cyclones and was located just south of the Nova Scotia coast (Fig. 3e). At $t = 0$ and +6 h, the trailing cold front remained just west of CYYT as the sea level cyclone moved northward into Labrador (Figs. 3f–h). Between $t = +6$ and +12 h, the trailing cold front (Figs. 3h–i) moved through CYYT, coinciding with the surface wind shift to the west and a surface temperature drop.

In Fig. 4, a time series of radar imagery from the Holyrood, Newfoundland, radar is presented, with images every 6 h from $t = -18$ to +12 h. Figure 4 shows that light precipitation was present at CYYT at $t = -18$ h (Fig. 4a) and bands of heavy precipitation were located just west of CYYT at $t = -12$ h (Fig. 4b) and $t = -6$ h (Fig. 4c). At $t = 0$ h (Fig. 4d), heavy precipitation was located directly over the station, and by $t = +6$ h (Fig. 4e) the precipitation has moved east of the station, following the passage of the trailing cold front.

A 5-day backward-trajectory analysis was performed for MAG 1 at $t = 0$ h (see Milrad et al. 2010 for methodological details). Trajectories end at approximately 300, 500, and 700 hPa. In Milrad et al. (2010), most of the extreme cases fit into one of three types based on parcel origin: west, southwest, and south. This classification system was based on the majority of trajectories originating from a particular direction (south, southwest, and west). In a few cases in Milrad et al. (2010), the low- and midlevel trajectories originated from the source region in which the event was eventually classified (e.g., southwest), while some upper-level trajectories originated from the west. The latter type of evolution was evident in the case of MAG 1, where the lower-level parcels primarily originated from the Atlantic Ocean (south), the midlevel parcels from the Gulf of Mexico (southwest), and the upper-level parcels from both the west and southwest (Fig. 5). In following Milrad et al. (2010), since

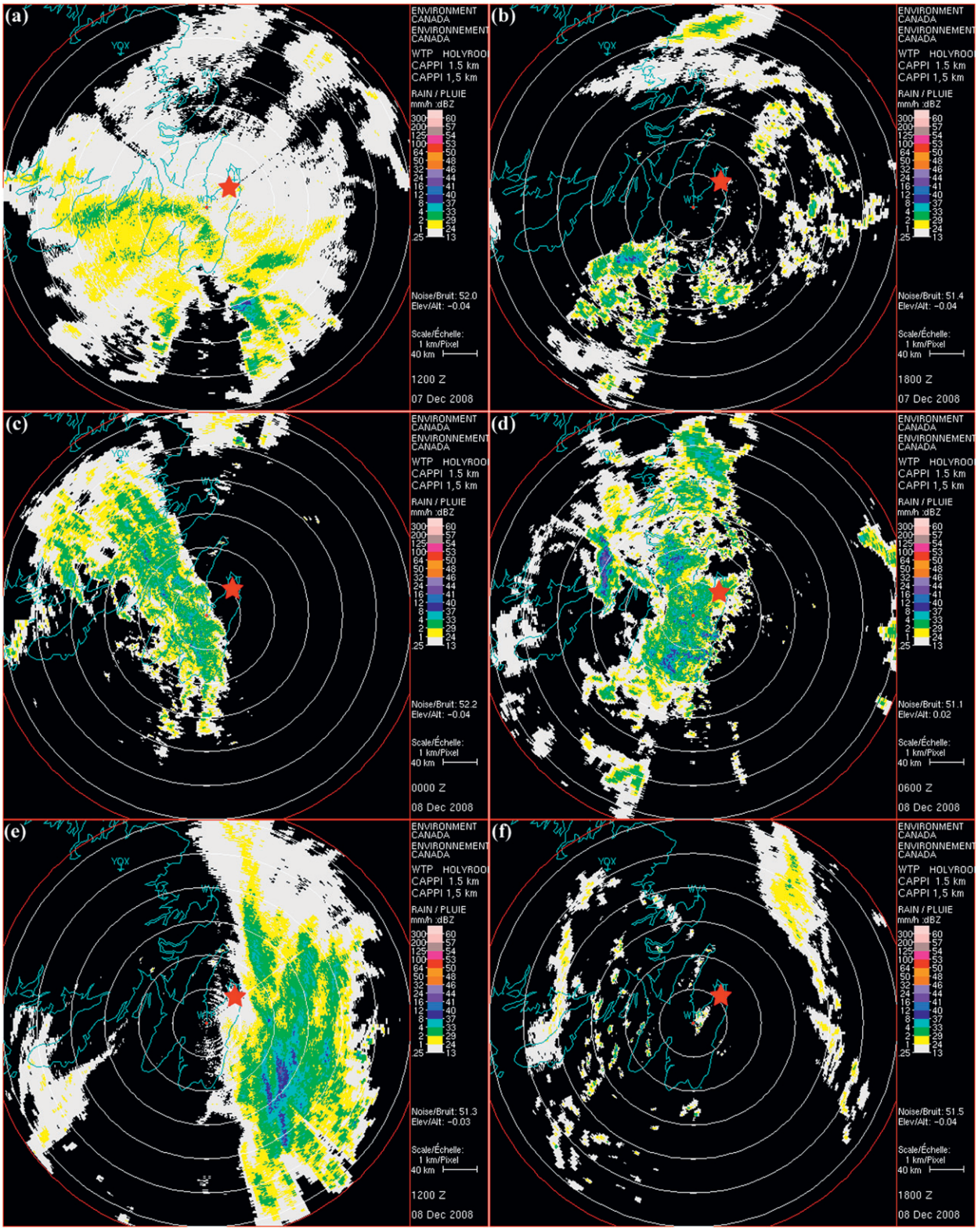

FIG. 4. Time series of radar imagery for MAG 1, from the Environment Canada radar located in Holyrood, Newfoundland. Radar imagery is shown for t = (a) −18, (b) −12, (c) −6, (d) 0, (e) +6, and (f) +12 h, where t = 0 h is 0600 UTC 8 Dec 2008. A red star is placed at the approximate location of CYYT.

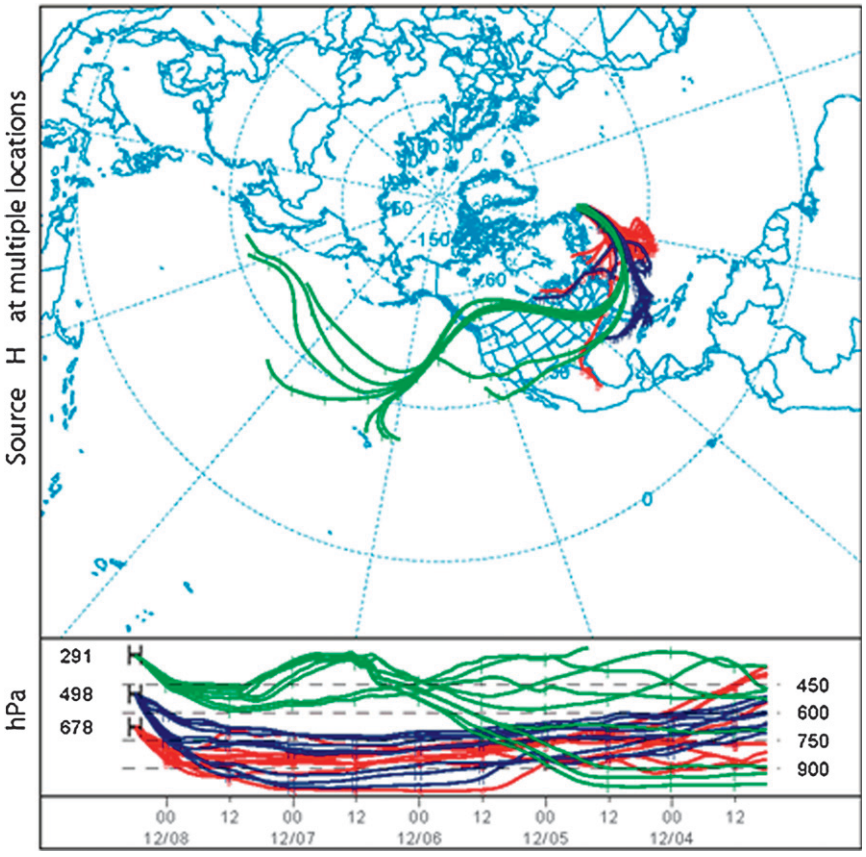

FIG. 5. Twenty-seven backward trajectories for MAG 1, derived from the NCEP GFS 1/2° analysis, with the origin being 5 days earlier and the ending points at 300, 500, and 700 hPa at 0600 UTC 8 Dec 2008. Ending points are distributed within a box whose corners are 48.4°N, 53.5°W and 46.4°N, 51.5°W.

the majority of the trajectories originate in the Gulf of Mexico, MAG 1 is classified as a southwest event.

A time series of three dynamically relevant QG ascent-forcing parameters from the NCEP–NCAR Global Reanalysis is displayed in Fig. 6a, based on the partitioning method of Milrad et al. (2010). Both the geostrophic and real-wind 1000–700-hPa frontogenesis results are shown in Fig. 6a following Milrad et al. (2010) to show that the two parameters exhibit the same general time evolution. The evolution of MAG 1 in Fig. 6a was in general agreement with the ''cyclone'' cases in Milrad et al. (2010), such that the values of the 1000–700-hPa horizontal temperature advection and 1000–700-hPa frontogenesis were relatively high at CYYT at the start of the event but rapidly became less positive around $t = 0$ h, whereas the midlevel vorticity advection became positive after $t = 0$ h (Fig. 6). This suggests that a midlatitude cyclone passed just to the west of CYYT, such that a warm front moved through CYYT ahead of the sea level cyclone and was followed 12–36 h later by the passage of a trailing cold front and the approach of the associated upper-level trough. It should be noted that the largest magnitudes of QG forcing are at $t = -6$ h (Fig. 6a), not $t = 0$ h; the classification system in Milrad et al. (2010) was primarily designed to describe the large-scale flow pattern for use by an operational forecaster and is not necessarily designed to unequivocally assess the time of heaviest precipitation, although in most cases, the parameters do line up accordingly.

Figures 6b shows a time series of precipitable water over the course of MAG 1. It is evident that remarkably large values of precipitable water were present at CYYT from $t = -12$ to $+6$ h. In particular, at $t = 0$ h, in the middle of December at 47°N, the precipitable water value at CYYT was over 32 mm (Fig. 6b). This value of precipitable water is over 20 mm greater than the climatological (1971–2000) average at CYYT for the month of December (9.47 mm). In addition, the largest precipitable water anomaly observed in the extreme composite of Milrad et al. (2009) was +14 mm, which is still approximately 9 mm smaller than the maximum value observed during MAG 1 (Fig. 6b). However, while

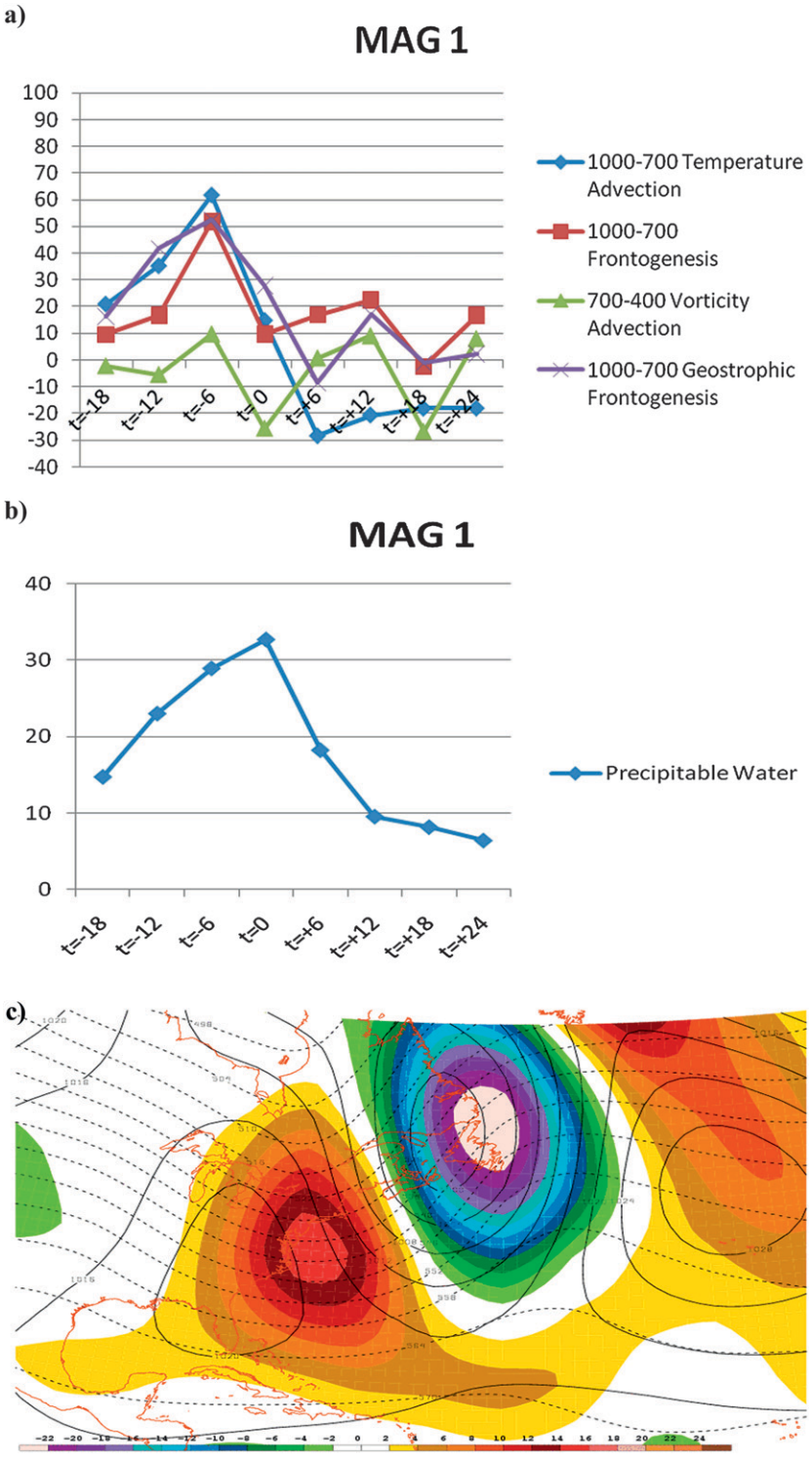

FIG. 6. Time series for MAG 1 during the period of precipitation at CYYT ($t = -18$ h, 1200 UTC 7 Dec, to $t = +24$ h, 0600 UTC 9 Dec), from the NCEP–NCAR Global Reanalysis for (a) 700–400-hPa layer-averaged relative vorticity advection $\times 10^{-10}$ s^{-2} (green), 1000–700-hPa layer-averaged horizontal temperature advection $\times 10^{-5}$ K s^{-1} (blue), 1000–700-hPa layer-averaged frontogenesis $\times 10^{-2}$ K (100 km)$^{-1}$ (3 h)$^{-1}$ (red), and 1000–700-hPa layer-averaged geostrophic frontogenesis $\times 10^{-2}$ K (100 km)$^{-1}$ (3 h)$^{-1}$ (purple); (b) column PW (mm, blue); and (c) 850–500-hPa layer-averaged omega (shaded cool colors for ascent) $\times 10^{-4}$ μPa s^{-1}.

it is greater than the average extreme event, the precipitable water value observed at CYYT is not climatologically unheard of. In following with the method of Hart and Grumm (2001), it is found that the precipitable water value observed during MAG 1 is approximately 1.5 standard deviations above the climatological mean.

Figure 6c shows the NCEP–NCAR Global Reanalysis 850–500-hPa layer-averaged vertical motion (ω), while Fig. 7 shows a time series of NCEP–NCAR Global Reanalysis $\mathbf{Q}_s$ (Figs. 7a, 7c, and 7e) and $\mathbf{Q}_n$ (Figs. 7b, 7d, and 7f) divergence. As previously discussed by Keyser et al. (1988) and Milrad et al. (2010), $\mathbf{Q}_s$ and $\mathbf{Q}_n$ are the along- and across-isentrope components of the $\mathbf{Q}$ vector, are proportional to the corresponding components of frontogenesis, and are defined by Eqs. (5) and (6), respectively, in Milrad et al. (2010). They are related to quasigeostrophic ascent via the $\mathbf{Q}$-vector form of the quasigeostrophic omega equation [Eq. (4) in Milrad et al. (2010)]. Keyser et al. (1988), albeit in a study of idealized atmospheric flows, suggested that $\mathbf{Q}_s$ is related to forcing from temperature advection as a result of a synoptic-scale wave, while $\mathbf{Q}_n$ relates to mesoscale forcing.

In the case of MAG 1, Figs. 7a, 7c, and 7e show that there was substantial $\mathbf{Q}_s$ convergence in association with the approaching sea level cyclone during the period in which 52 mm of the 73.6 mm of precipitation was recorded at CYYT ($t = -12$ to $+6$ h). At $t = -12$ and -6 h, $\mathbf{Q}_n$ convergence was also present (Figs. 7b and 7d), albeit smaller in magnitude than the $\mathbf{Q}_s$ convergence. This implies that the majority of the forcing for ascent was in conjunction with the synoptic-scale warm-air advection associated with the sea level cyclone discussed in section 3b. However, the fact that $\mathbf{Q}_n$ convergence was observed at both $t = -12$ and -6 h suggests that mesoscale frontogenetical forcing for ascent plays a more substantial role during part of MAG 1 than in the cyclone group composite members of Milrad et al. (2010), although certainly less so than in MAG 2 (section 4a). This is not the case at $t = 0$ h, where substantial $\mathbf{Q}_s$ convergence is observed (Fig. 7e) alongside $\mathbf{Q}_n$ divergence.

b. Synoptic–dynamic analysis

It was shown in section 3a that MAG 1 produced 73.6 mm of precipitation. Satellite imagery demonstrated that this extreme event was associated with an intensifying sea level cyclone approaching St. John's from the south and west. In this section, the dynamics of the cyclone as well as the thermodynamics of the air mass at CYYT are analyzed.

Two days prior to the heaviest precipitation at CYYT ($t = -48$ h), and in association with an upper-level trough, a weak sea level cyclone is located over the northern Great Lakes (Fig. 8a), which proceeds to propagate eastward and be situated near Lake Ontario at $t = -24$ h (Fig. 8b). By $t = -24$ h (Fig. 8b), the trough on the DT, defined here as the 2-PVU surface, where 1 potential vorticity unit (PVU) = 10^{-6} m^2 s^{-1} K kg^{-1}, approaches the eastern seaboard of the United States. Concurrently, a secondary area of low pressure develops off the North Carolina coast (Fig. 8b). At $t = -12$ h (Fig. 8c), the initial sea level cyclone over the Great Lakes disappears and is replaced by a 992-hPa sea level cyclone off the eastern seaboard. The trough on the DT is now located southwest of the developing sea level cyclone, as the system establishes a westward tilt with height. From the initial sea level cyclone development at $t = -24$ h (1008 hPa; Fig. 8b) to its position just west of CYYT at $t = 0$ h (980 hPa; Fig. 8e), the cyclone intensifies by 28 hPa, surpassing the "bomb" criterion established by Sanders and Gyakum (1980). By $t = +12$ h, after the trailing cold front has passed through CYYT, the cyclone center is located northeast of Labrador, with a minimum sea level pressure of 968 hPa, completing a 50-hPa intensification in 36 h.

At $t = 0$ h, as the sea level cyclone passed just west of the station, high values of θ on the DT are located over CYYT (Fig. 8e). In fact, the values of θ near CYYT steadily increase from $t = -36$ h (not shown) until the passage of the trailing cold front between $t = +6$ and $+12$ h (Fig. 8f), and are quantitatively similar to values observed over the southern United States and Gulf of Mexico. The extremely warm DT at CYYT, while the station is in the warm sector of the cyclone, suggests the presence of a subtropical air mass. In addition, it is implied that the downstream ridge on the DT intensifies from $t = -24$ h (Fig. 8b) to $t = +6$ h (Fig. 8f) due to (a) strong low-level warm-air advection ahead of the sea level cyclone and (b) latent heat release as a result of the heavy precipitation seen in Figs. 4b–d. This is consistent with the findings of Milrad et al. (2009, 2010) for the extreme and cyclone group composites, respectively.

MAG 1 is a classic case of rapid East Coast cyclogenesis; however, the climatology of Milrad et al. (2009) shows that 70+ mm of precipitation at CYYT during one precipitation event has occurred only 5 times in the past 30 yr. Therefore, it is likely that the extreme precipitation as a result of MAG 1 is due to a potent combination of a myriad of factors. While it is established that large amounts of QG forcing for ascent (low-level warm-air advection and low-level frontogenesis) are present at CYYT from $t = -18$ to -6 h (Fig. 6a), both moisture availability and the thermodynamic properties of the air mass at CYYT during this time period are also crucial in explaining the amount of precipitation.

Warm moist air at CYYT, on the east side (warm sector) of the rapidly intensifying cyclone, is shown by

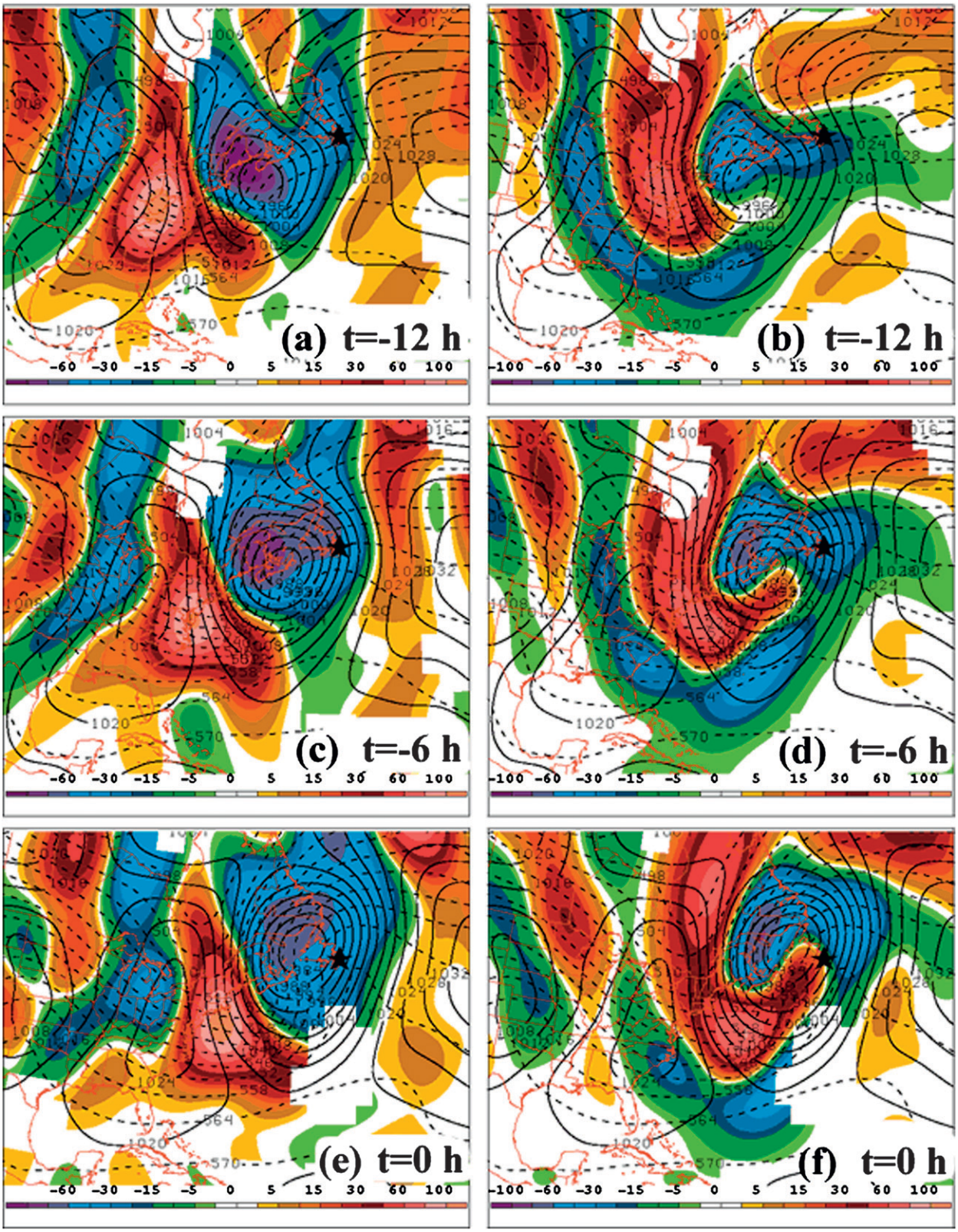

FIG. 7. For MAG 1, NCEP–NCAR Global Reanalysis plots of (left) 850–500-hPa layer-averaged $\mathbf{Q}_s$ and (right) $\mathbf{Q}_n$ divergence $\times 10^{-17}$ K m^{-2} s^{-1}, from t = (a),(b) −12, (c),(d) −6, and (e),(f) t = 0 h. Cool (warm) colors represent convergence (divergence).

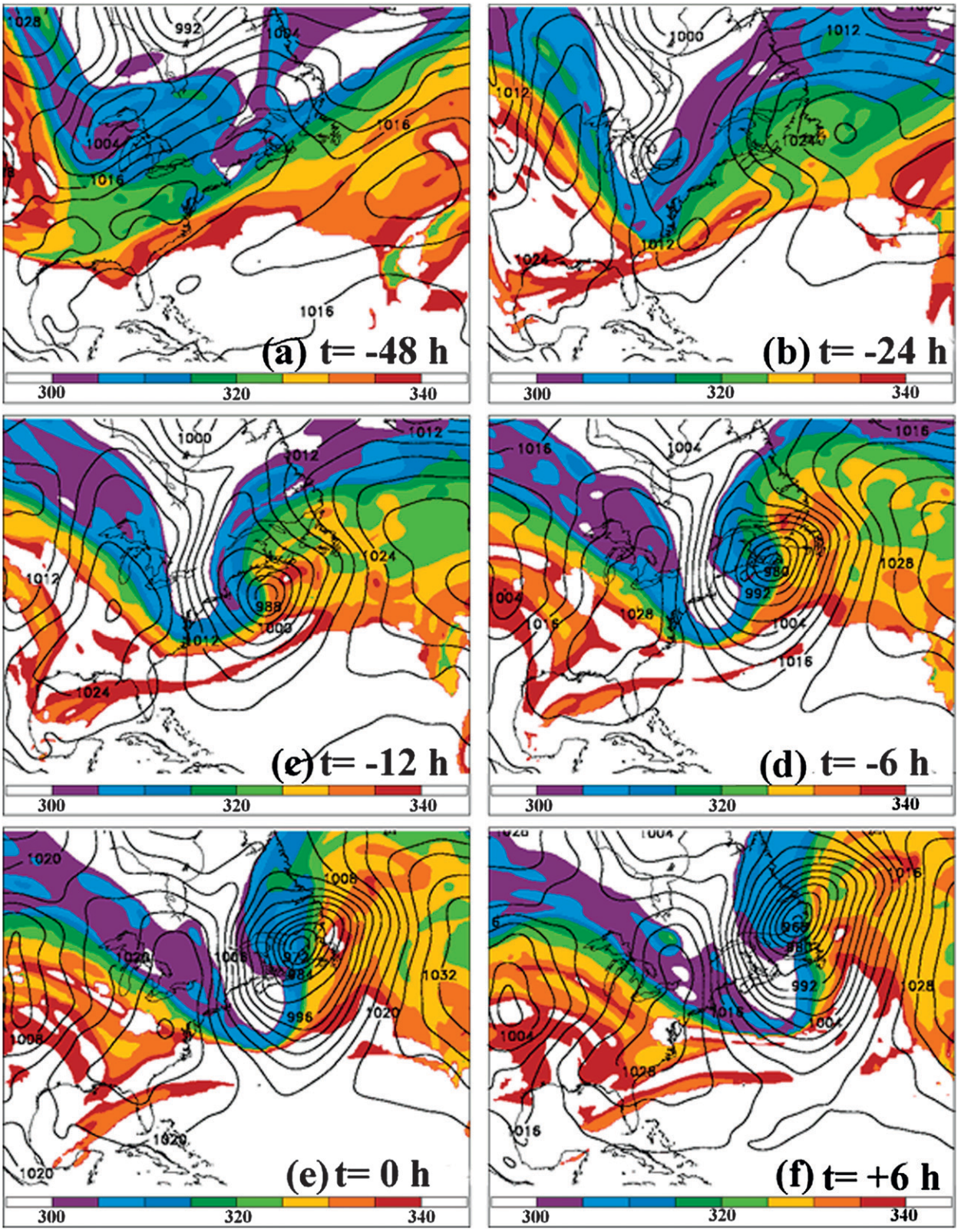

FIG. 8. Time series of GFS 1/2° analysis sea level pressure (SLP, solid) contoured every 4 hPa, and potential temperature (K) on the dynamic tropopause (2-PVU surface, shaded), for MAG 1. Results are shown for t = (a) −48, (b) −24, (c) −12, (d) −6, (e) 0, and (f) t = +6 h, where t = 0 h is 0600 UTC 8 Dec 2008.

the presence of large values of equivalent potential temperature (θ_e) at 850 hPa (Fig. 9). These θ_e values are greater than those present in the Gulf of Mexico, as a plume of moist subtropical air extends from near Bermuda northward to Atlantic Canada from $t = -12$ to $+6$ h (Figs. 9c–f), before finally moving east of Newfoundland after $t = +6$ h (Fig. 9f), as the sea level cyclone propagates away.

The coupling index (CI), a measure of the bulk atmospheric stability, was used by Bosart and Lackmann (1995), Roebber and Gyakum (2003), and Galarneau and Bosart (2006) as θ on the DT minus the low-level θ_e. Here, the DT is the 2-PVU surface and the low-level θ_e is taken at 850 hPa (Galarneau and Bosart 2006). Figures 9d–f shows that an area of relatively low CI (<8 K) approaches CYYT from the southwest, concomitant with the highest values of 850-hPa θ_e. The authors believe the gradient in CI evident near and just east of CYYT at $t = 0$ h (Fig. 9e) supports the assertion that the warm, moist sector (high θ_e) of the cyclone moves east of St. John's shortly after $t = 0$ h and before $t = +6$ h (the period of heaviest precipitation). After $t = +6$ h, the area of low CI moves well east of CYYT as the trailing cold front ushers in more stable air from the west, concomitant with lesser amounts of precipitation at the end of the event.

Figure 10 displays the 1000–700-hPa moisture transport vectors and associated moisture flux divergence. Even before the development of the sea level cyclone off the North Carolina coast at $t = -24$ h (Fig. 10b), substantial moisture transport from the Atlantic Ocean and Gulf of Mexico is present on the western side of the downstream anticyclone. As the sea level cyclone develops and rapidly intensifies, the moisture transport on the eastern flank of the cyclone increases, resulting in a broad area of moisture convergence at CYYT from $t = -12$ to 0 h (Figs. 10c–e).

Figure 11 displays a time series of observed soundings taken every 12 h at CYYT. As the rapidly intensifying cyclone moves toward CYYT and subtropical moisture is advected northward, the atmosphere quickly saturates by $t = -18$ h (Fig. 11b). From $t = -18$ h (Fig. 11b) to $t = +6$ h (Fig. 11d), the tropopause remains extremely elevated (near 200 hPa), and nearly saturated, supporting the earlier observation that a warm moist air mass exists at CYYT ahead of the sea level cyclone. Following the passage of the trailing cold front and the approach of the main upper-level disturbance between $t = +6$ and $+12$ h, the thermodynamic structure of the atmosphere shifts quickly to one with a depressed tropopause of around 400 hPa at $t = +18$ h (Fig. 11e) and 500 hPa at $t = +30$ h, and much lower temperature and mixing ratio values. This illustrates the stark difference in the air mass on either side of the trailing cold front and suggests that the bulk of the precipitation during MAG 1 fell during a period marked by strong QG forcing for ascent in the presence of a warm moist air mass.

Emanuel (1983) stated that conditional symmetric (slantwise) instability (CSI) can be largely responsible for some mesoscale precipitation bands within larger-scale storms. Schultz and Schumacher (1999) presented an ingredients-based methodology for forecasting slantwise convection, the components of which are moisture, lift, and instability. Since it has already been established in this section that there was substantial moisture and forcing for ascent, a check for both slantwise and gravitational instability is presented is Fig. 12. Figure 12 displays negative (shaded) values of saturated equivalent geostrophic potential vorticity (MPV_g^*), defined as the criterion for CSI by Schultz and Schumacher (1999) along with saturated equivalent potential temperature. The cross section is roughly perpendicular to the thermal wind, although Schultz and Schumacher (1999) point out that MPV_g^* is much less sensitive to the orientation of the cross sections than momentum (M) surfaces. Finally, regions of vertical convective instability ($d\theta_e/dz < 0$; Bluestein 1992) can often be collocated with CSI (Schultz and Schumacher 1999). However, the convective instability mode may dominate a situation where both types of instability are present (Emanuel 1983).

Figure 12 shows that the criterion for CSI ($\mathrm{MPV}_g^* < 0$) in the vicinity of CYYT is satisfied from $t = -6$ to $+12$ h. Since the majority of the event precipitation fell before $t = +6$, the focus is on Figs. 12c–e. In Fig. 12c, an area of weak CSI is observed in the 800–500-hPa layer, in the vicinity of CYYT. This area has expanded eastward and upward from its location at $t = -12$ h (Fig. 12b). By $t = 0$ h (Fig. 12d), the region of CSI is located in the lowest 300 hPa of the troposphere and the value of MPV_g^* is more negative than at previous times. Additionally, there is a region of convective instability present near 850 hPa (Fig. 12d). This suggests that at $t = 0$ h, both gravitational and symmetric instabilities are present, supporting the assertions of Schultz and Schumacher (1999) that regions of CSI are often observed prior to the development of convective instability, and that it is not uncommon to observe both instabilities simultaneously. The Holyrood radar imagery (Figs. 4c–e) lends credence to this idea in showing banded precipitation structures over Newfoundland at $t = -6$ h (Fig. 4c), more cellular structures at $t = 0$ h (Fig. 4d), and banded precipitation at $t = +6$ h (Fig. 4e). Accordingly, at $t = +6$ h, just prior to the passage of the surface cold front, the region of CSI is still present, located in the lowest 150 hPa, while the area of convective instability has dissipated.

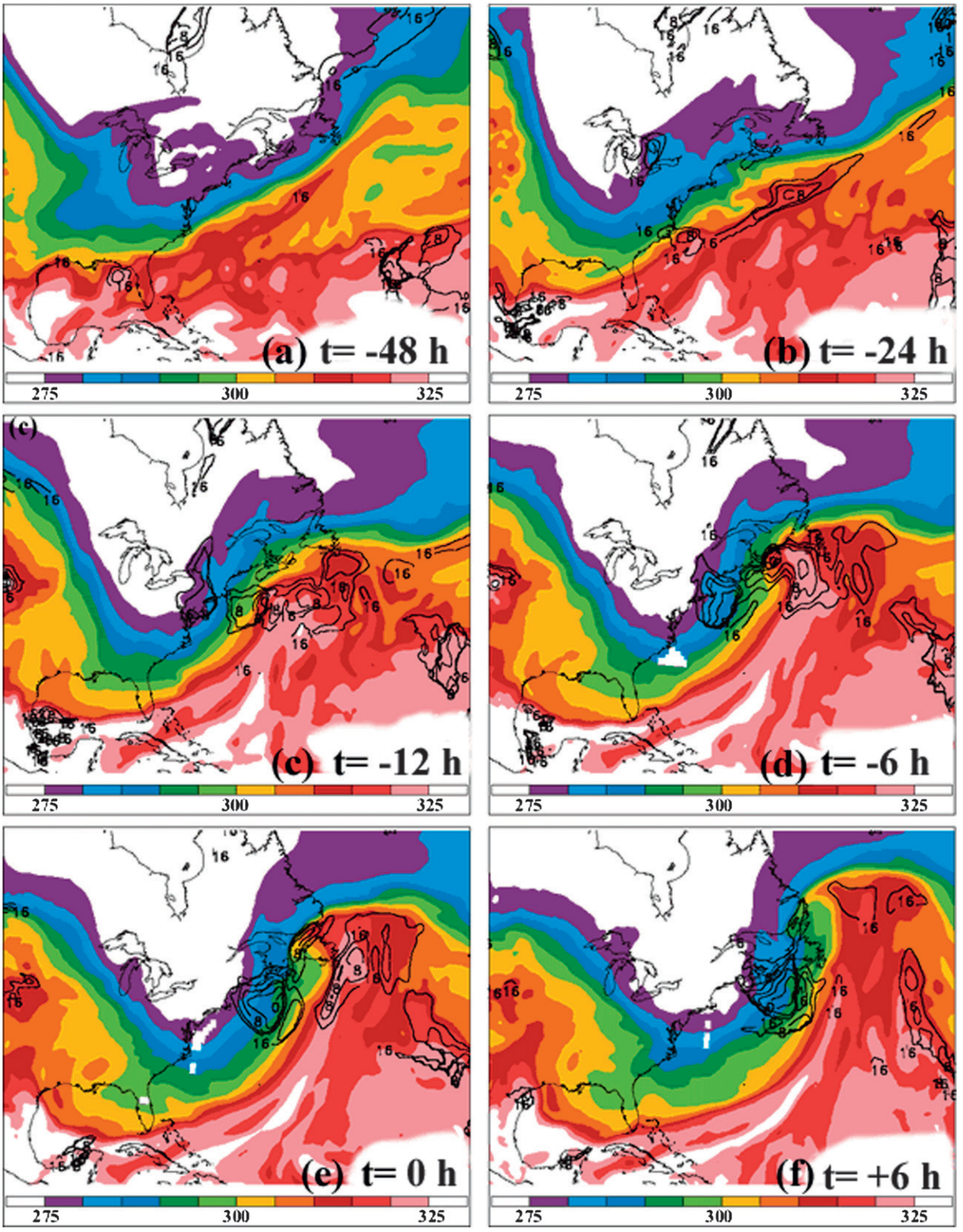

FIG. 9. As in Fig. 8, but for 850-hPa equivalent potential temperature (K, shaded) and CI (solid, every 4 K from 0 to +16).

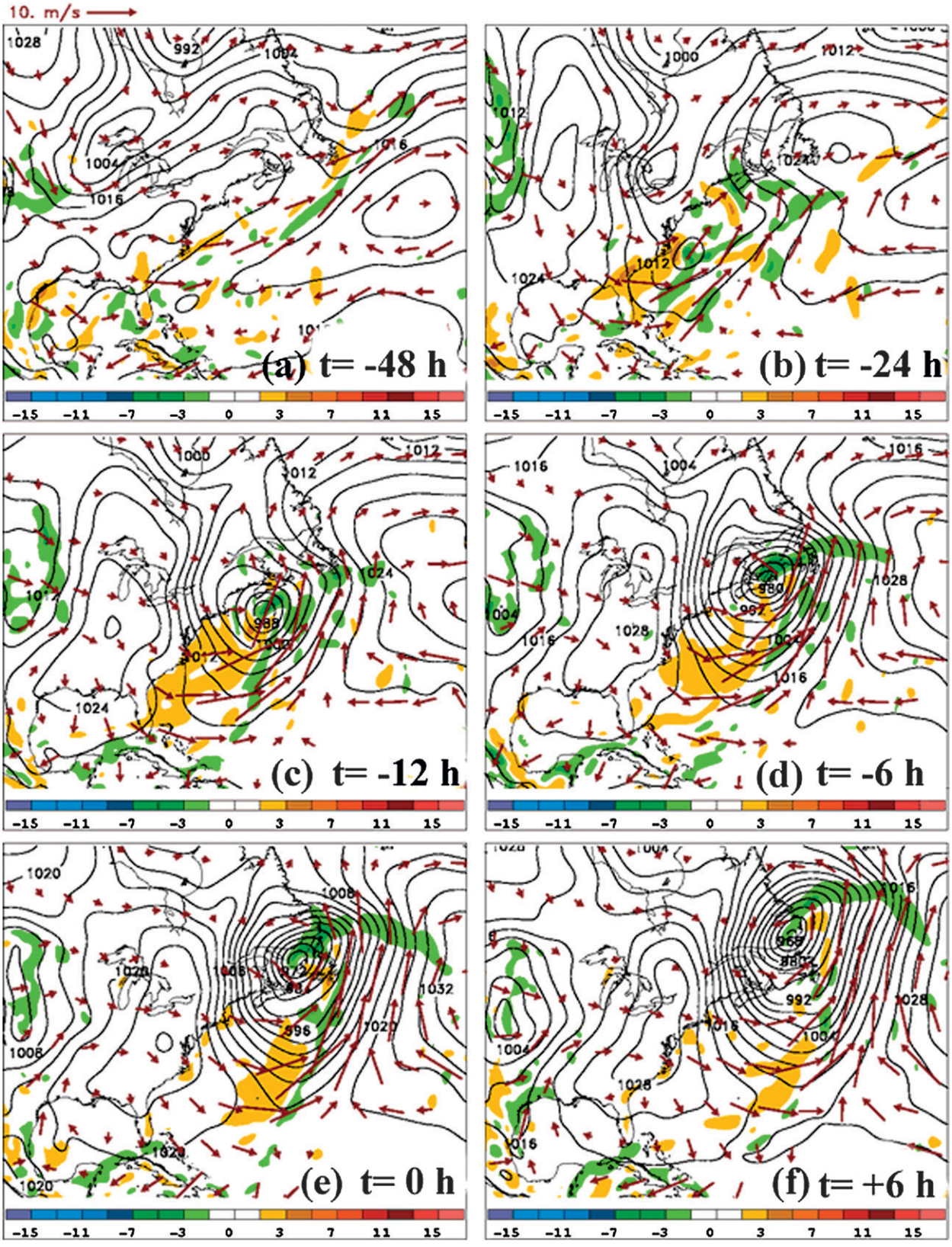

FIG. 10. As in Fig. 8, but for SLP (solid, every 4 hPa), 1000–700-hPa moisture flux convergence ($\times 10^{-8}$ kg m^{-2} s^{-1}, shaded), and 1000–700-hPa moisture transport vectors (g kg^{-1} m s^{-1}, red), with reference vector in the top left-hand corner.

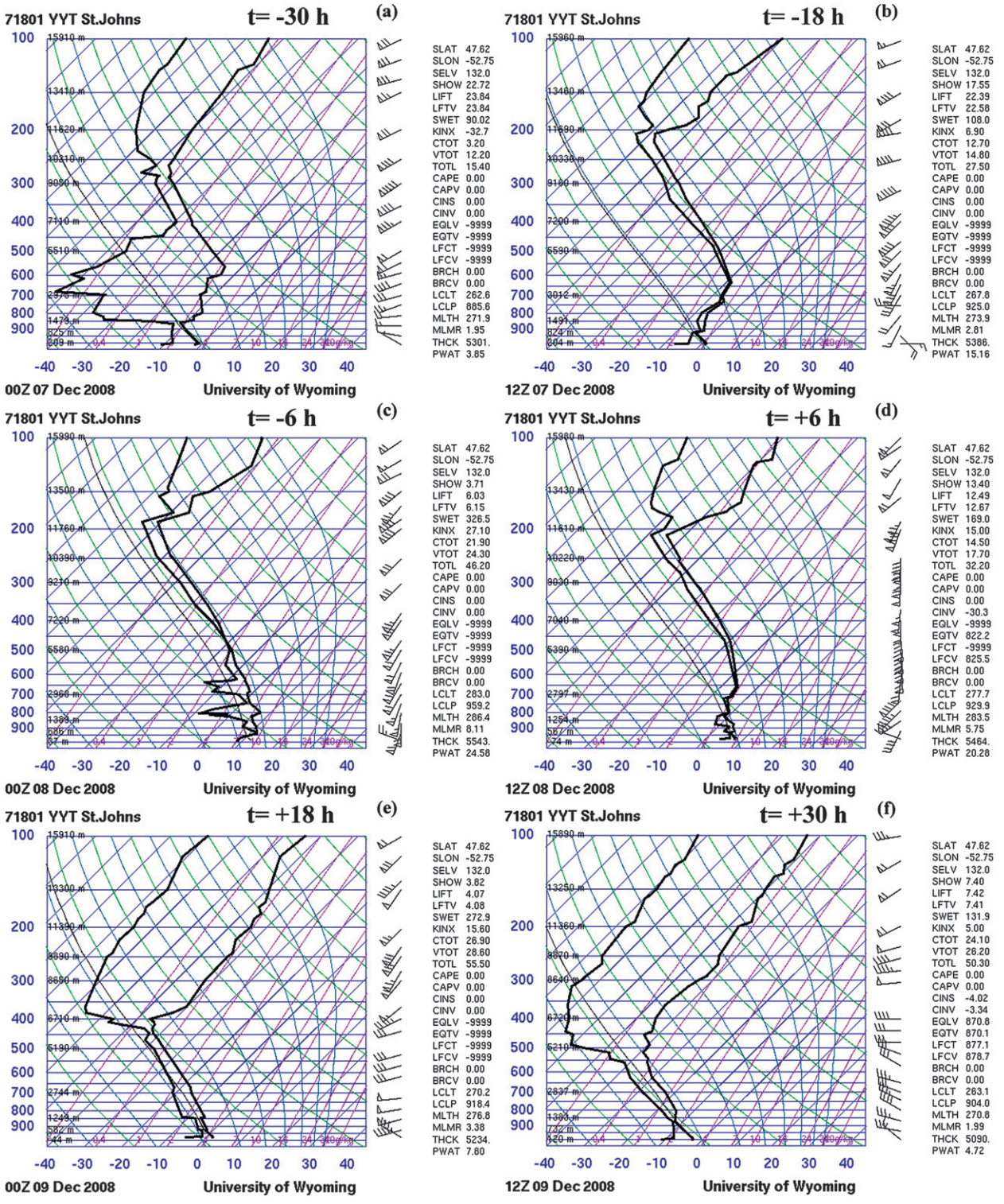

FIG. 11. Time series of observed soundings at CYYT for MAG 1. Soundings are shown for t = (a) −30, (b) −18, (c) −6, (d) +6, (e) +18, and (f) t = +30 h, where t = 0 h is 0600 UTC 8 Dec 2008.

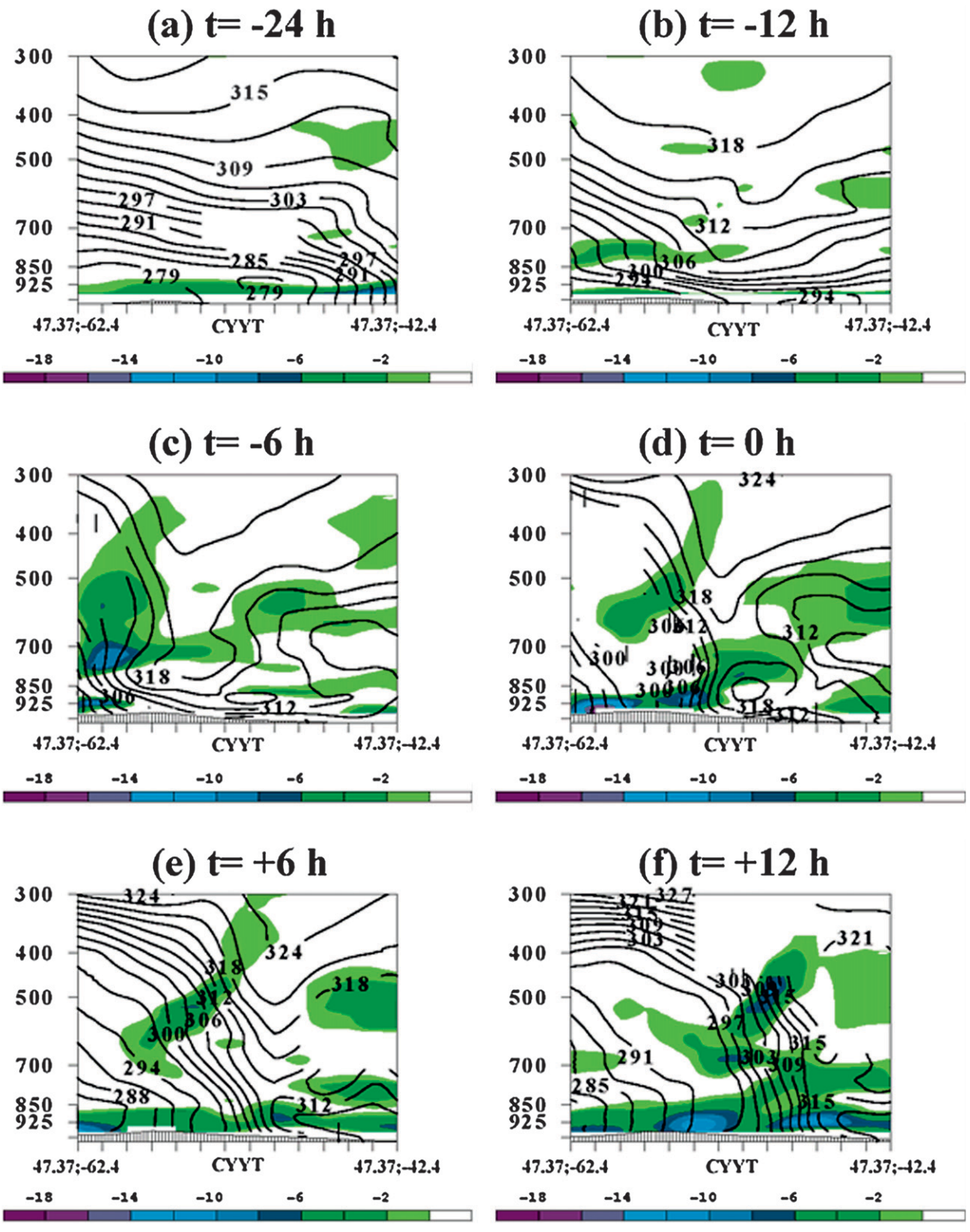

FIG. 12. Time series of cross-section plots along latitude 47.37°N, from −62.4°W to −42.4°W, for MAG 1. Saturated equivalent geostrophic potential vorticity ($\times 10^{-7}$ m^2 s^{-1} K kg^{-1}, shaded for negative values), equivalent potential temperature (K, contoured) shown for t = (a) −24 h, (b) −12, (c) −6, (d) 0, (e) +6, and (f) t = +12 h, where t = 0 h is 0600 UTC 8 Dec 2008. The location of CYYT is marked in each panel.

4. MAG 2: 11 December 2008

a. Overview and synoptic typing

MAG 2 affected CYYT from 0000 UTC 11 December to 0000 UTC 13 December, with $t = 0$ h at 0600 UTC 11 December. The total amount of precipitation observed at CYYT was 54 mm (Fig. 13), which is approximately 10 mm above the median extreme event defined in Milrad et al. (2009). MAG 2 occurred in three stages: an initial warm stage, a subsequent cold stage following a cold-frontal passage, and a second warm stage, as a quasi-stationary northeast–southwest-oriented baroclinic zone retreated back to the north of CYYT ahead of an approaching cyclone. Over half of the total event precipitation fell during the initial warm stage and subsequent cold frontal passage (Fig. 13), between 0000 and 1200 UTC 11 December. During this time period, unseasonably warm surface temperatures close to 15°C were replaced by a much cooler yet still saturated atmosphere (Fig. 13a). Accompanying the temperature drop between 0600 and 1200 UTC ($t = 0$ and $+6$ h) 11 December was a wind shift from 20-kt (10.29 m s^{-1}) westerly surface flow to 10-kt (5.14 m s^{-1}) northerly flow (Fig. 13a). While moderate rain was reported at several time periods during the initial warm period and subsequent frontal passage, the precipitation slowly transitioned to light frozen precipitation by $t = +12$ h and remained frozen until around $t = +27$ h when slowly rising surface temperatures caused a changeover to light rain. Toward the end of the event (Fig. 13b), cold boundary layer air remained in place until around 2100 UTC ($t = +39$ h) 11 December when the aforementioned boundary returned as a northward-moving warm front, initiating the second warm stage, ahead of a developing cyclone off the southeastern U.S. coast.

Figure 14 shows clouds associated with the baroclinic zone, stretching from northeastern Quebec to Louisiana at $t = -36$ h (Fig. 14c). The baroclinic zone slowly propagated eastward toward CYYT and, by $t = -6$ h (Fig. 14f), stretched from an area northeast of Newfoundland southwestward into the Gulf of Mexico. Slightly upstream of the frontal zone was a closed upper-level low over the western Gulf of Mexico (Figs. 14f–h and 18c–f) that impacted the later stages of MAG 2, as well as the subsequent few days along the Atlantic seaboard. Unfortunately, the Holyrood radar was not operating from $t = -10$ to $+12$ h, the time in which most of the precipitation fell during MAG 2.

As in MAG 1 (section 3a), the evolution of the backward trajectories was more complicated than most of the cases in Milrad et al. (2010). Figure 15 shows that some of the upper-level trajectories (300 hPa) originated southwest of CYYT to the Gulf of Mexico, while others traced backward initially to the Gulf of Mexico and then into the eastern Pacific. However, while some of the midlevel (500 hPa) trajectories also trace backward to the Gulf of Mexico, most of the mid- and low-level parcels spent a large amount of time over the Gulf Stream. In sum, MAG 2 is classified as a southwest event, with the caveat that the low-level trajectories originated in the upper troposphere early in the time evolution, over the American and Canadian prairies.

Figure 16a displays time series of QG ascent-forcing parameters. As in the 11 frontal cases in Milrad et al. (2010), the magnitude of low-level frontogenesis is large, while the magnitudes of the other two QG variables in the time series (Fig. 16a) are small, especially compared to cyclone events. In addition, the frontogenesis values observed for MAG 2 exceed those observed for MAG 1, which supports the findings of Milrad et al. (2010) in differentiating cyclone and frontal events. Finally, midlevel vorticity advection values near zero for the entire period of precipitation suggest that a strong upper-level trough did not come into play during the evolution of MAG 2; MAG 2 is categorized as a frontal case.

Figure 16b shows that during the entire period of precipitation (42 h) at CYYT, the precipitable water remains at 20 mm or above. The maximum precipitable water value (~28 mm) is at $t = 0$ h, coincident with the heaviest precipitation (21 mm). In following with Hart and Grumm (2001), values of precipitable water are approximately one standard deviation above the climatological mean, and slightly above the composite extreme event in Milrad et al. (2009). The observed long duration of high precipitable water (PW) values likely plays a role in the extreme amount of precipitation observed during MAG 2. Finally, Fig. 16c shows that at $t = 0$ h, there was ascent at St. John's (and along the length of the baroclinic zone), but it was relatively weak. This finding is consistent throughout MAG 2 (not shown), which is marked by relatively weak ascent in a favorable environment for heavy precipitation. This is discussed further in section 4b.

Figure 17 suggests that during the period of heaviest precipitation at CYYT ($t = -6$ to $+12$ h), when 35 mm of the total event's 54 mm was recorded, $\mathbf{Q}_n$ is substantially more convergent than $\mathbf{Q}_s$, as $\mathbf{Q}_s$ divergence is observed at both $t = 0$ and $+6$ h (Figs. 7c,e). This is consistent with the results for the frontal composite in Milrad et al. (2010) and suggests that mesoscale frontogenetical forcing is a much bigger player (relative to synoptic-scale frontogenesis) in MAG 2 than in MAG 1.

b. Synoptic–dynamic analysis

Figure 18 displays a downstream ridge on the DT, similar to the frontal composite of Milrad et al. (2010). Prior to MAG 2, as the intense sea level cyclone

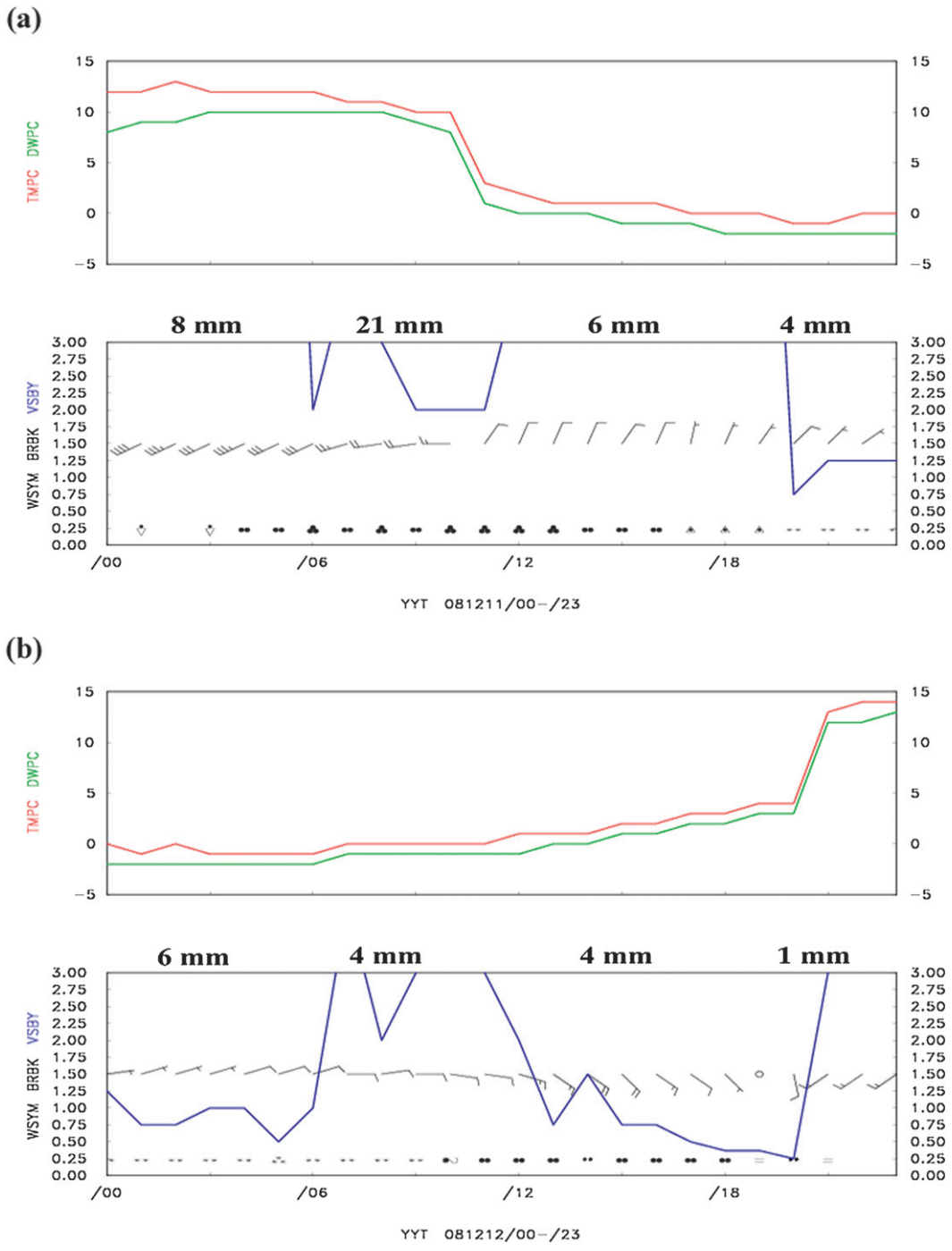

FIG. 13. Meteograms for the entire period of precipitation at CYYT for MAG 2. As in Fig. 2, but for (a) 11 Dec and (b) 12 Dec 2008.

responsible for MAG 1 moved away from Newfoundland, the associated upper-level trough moves over Newfoundland at $t = -48$ h (Fig. 18a). By $t = -24$ h, the sea level anticyclone is established downstream of CYYT and potentially cold air aloft is replaced by high θ on the DT, advected by strong southerly flow in association with the downstream anticyclone and a closed upper-level low in the western Gulf of Mexico (Fig. 18b).

The assertion that MAG 2 was a three-stage event is supported by Fig. 18, which shows warm θ on the DT prior to $t = +6$ h (Figs. 18a–e), replaced by cooler θ at $t = +6$ h (Fig. 18f). By $t = +12$ h, however, the high-θ air

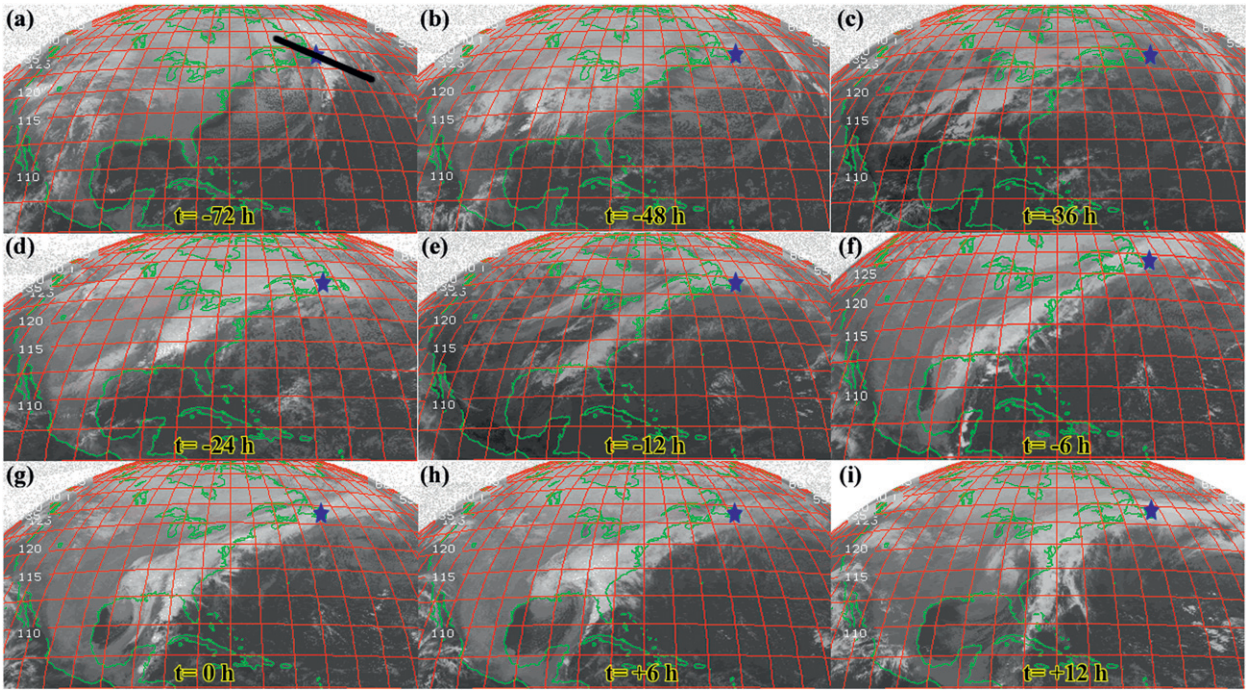

FIG. 14. Time series of infrared satellite imagery for MAG 2. Images are presented for (a) $t-72$, (b) -48, (c) -36, (d) -24, (e) -12, (f) -6, (g) 0, (h) $+6$, and (i) $+12$ h, where $t = 0$ h is 0600 UTC 11 Dec 2008. A blue star is placed in each panel at the approximate location of CYYT and the area of interest explored in Fig. 20 (cross section) is outlined with a black line in (a).

returns as the surface baroclinic zone retreats northward in association with the developing cyclone in the Gulf of Mexico (not shown). By $t = +24$ h (not shown), the baroclinic zone is fully to the north of CYYT and the station remains in the subtropical air mass until the passage of the Gulf of Mexico cyclone on 13 December.

Figure 19 highlights a plume of warm low-level θ_e extending parallel to the baroclinic zone from the Gulf of Mexico to northeast of Newfoundland. Figure 19 also confirms that the bulk atmospheric stability in MAG 2 is substantially higher than in MAG 1. While there are low (<8 K) values of the CI observed off the U.S. coast on the southern edge of the baroclinic zone, the lowest values do not make it into the CYYT area, even at $t = 0$ h (Fig. 19e).

Figure 20b highlights the fact that strong moisture transport on the western flank of the downstream high is already established by $t = -24$ h. This northward moisture transport continues unabated for more than 48 h, with the largest vectors and a persistent area of moisture convergence located over CYYT (Fig. 20). The relatively long duration of the moisture transport convergence and the high precipitable water values are likely important factors in the extreme amount of precipitation during MAG 2.

Figure 21 shows that the tropopause remains very high, hovering between 150 and 200 hPa during the $t = -6$ to $+42$-h time period. Unlike in MAG 1, the tropopause remains high for the duration of the precipitation period during MAG 2, suggesting that there was no drastic shift in air mass during the event. However, Figs. 21c–e show a shallow layer of cold air in the lower tropopause following the initial cold frontal passage; this cold air remains only in the boundary layer with a 200–300-hPa inversion layer situated above it. This supports the previously discussed cool surface temperatures following the initial cold front passage (Fig. 13).

Figure 22 displays cross-section plots oriented northwest–southeast, roughly perpendicular to the quasi-stationary baroclinic zone (Fig. 14). Over 60% of the precipitation during MAG 2 fell between $t = -6$ and $+12$ h. However, there was a region of CSI near CYYT, in the near-surface layer, prior to precipitation falling, at $t = -24$ h (Fig. 22a) and $t = -12$ h (Fig. 22b). This area is persistent through $t = -6$ h (Fig. 22c) and $t = 0$ h (Fig. 22d), with stronger values located to the northwest of CYYT. At $t = 0$ h (Fig. 22d), there is also a small region of convective instability around 850 hPa, in the vicinity of CYYT, which translates eastward by $t = +6$ h (Fig. 22e) and $t = +12$ h (Fig. 22f). Consequently, it appears that convective-symmetric instability was present near CYYT at $t = 0$ h, as was observed during MAG 1, while CSI was present during most of the heaviest precipitation period. The presence of CSI (and

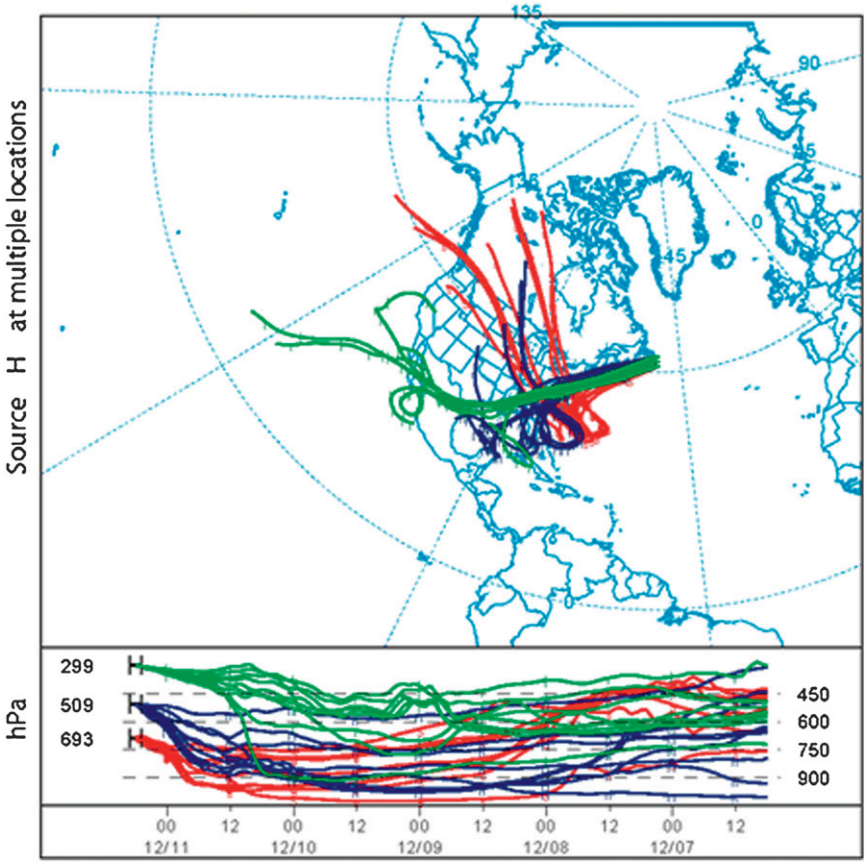

FIG. 15. Twenty-seven backward trajectories for MAG 2 derived from the NCEP GFS 1/2° analysis, with the origin being 5 days earlier and the ending points at 300, 500, and 700 hPa at 0600 UTC 11 Dec 2008. Ending points are distributed within a box whose corners are 48.4°N, 53.5°W and 46.4°N, 51.5°W.

short-lived convective instability) helped to allow for the development of heavy precipitation in the presence of frontogenetical forcing for ascent, a process that is fairly common (Schultz and Schumacher 1999).

5. Concluding discussion and future work

Analyses are presented for consecutive extreme precipitation events that produced over 125 mm of precipitation at CYYT from 7 to 12 December 2008 (Fig. 2). The first case, MAG 1, was associated with a rapidly intensifying extratropical cyclone that tilted westward with height (Fig. 8). The synoptic typing of Milrad et al. (2010) was utilized, and MAG 1 was classified as a southwest and cyclone event. The extreme amount of precipitation as a result of MAG 1 was associated with large values of QG forcing for ascent (Fig. 6a) in the presence of weak stability (Fig. 9) and an extremely moist subtropical air mass (Figs. 8 and 12). Both CSI and convective instability were present near CYYT at $t = 0$ h (Fig. 12d). As soon as the cyclone passed CYYT, there was a drastic shift in air mass (Fig. 11), as the tropopause descended from near 200 hPa at $t = +6$ h to around 400 hPa at $t = +12$ h.

MAG 2, which produced 54 mm of precipitation, was primarily associated with a quasi-stationary northeast–southwest baroclinic zone near CYYT (Fig. 20). MAG 2 is classified as a southwest and frontal event. Unlike in MAG 1, there was no evidence of a strong extratropical cyclone near CYYT during the period of precipitation of MAG 2. The bulk of the precipitation during MAG 2 was associated with large values of low-level frontogenesis (Fig. 16a) in the presence of relatively large, persistent values of precipitable water, and regions of CSI and convective instability at $t = 0$ h (Fig. 22d).

Consistent with the composite analysis of frontal events in Milrad et al. (2010), the synoptic environment during MAG 2 was dominated by a downstream upper-level ridge and corresponding sea level anticyclone (Figs. 20 and 21). Although approximately 40% of the

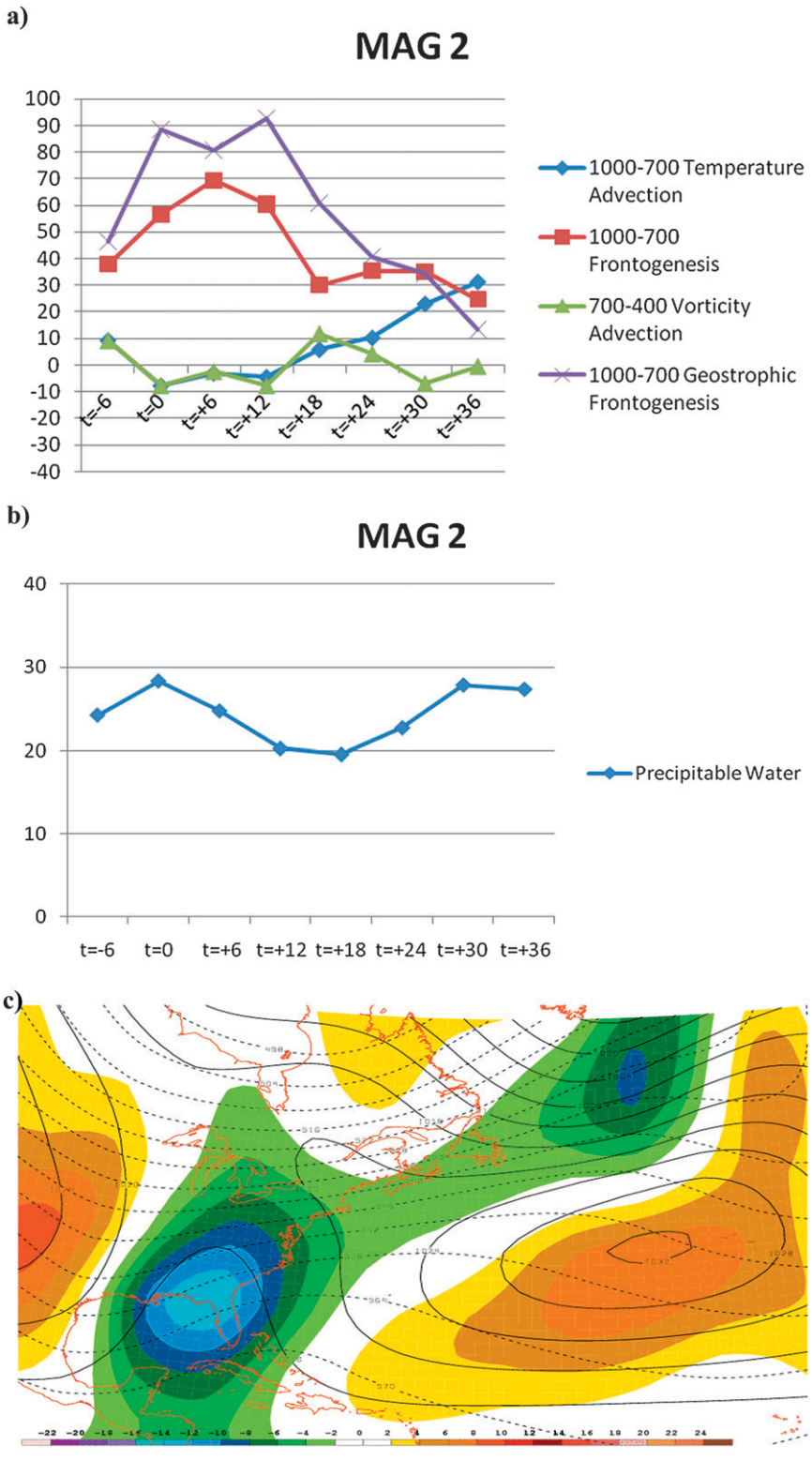

FIG. 16. As in Fig. 6, but for MAG 2 during the period of precipitation at CYYT ($t = -6$ h, 0000 UTC 11 Dec, to $t = +36$ h, 1800 UTC 12 Dec).

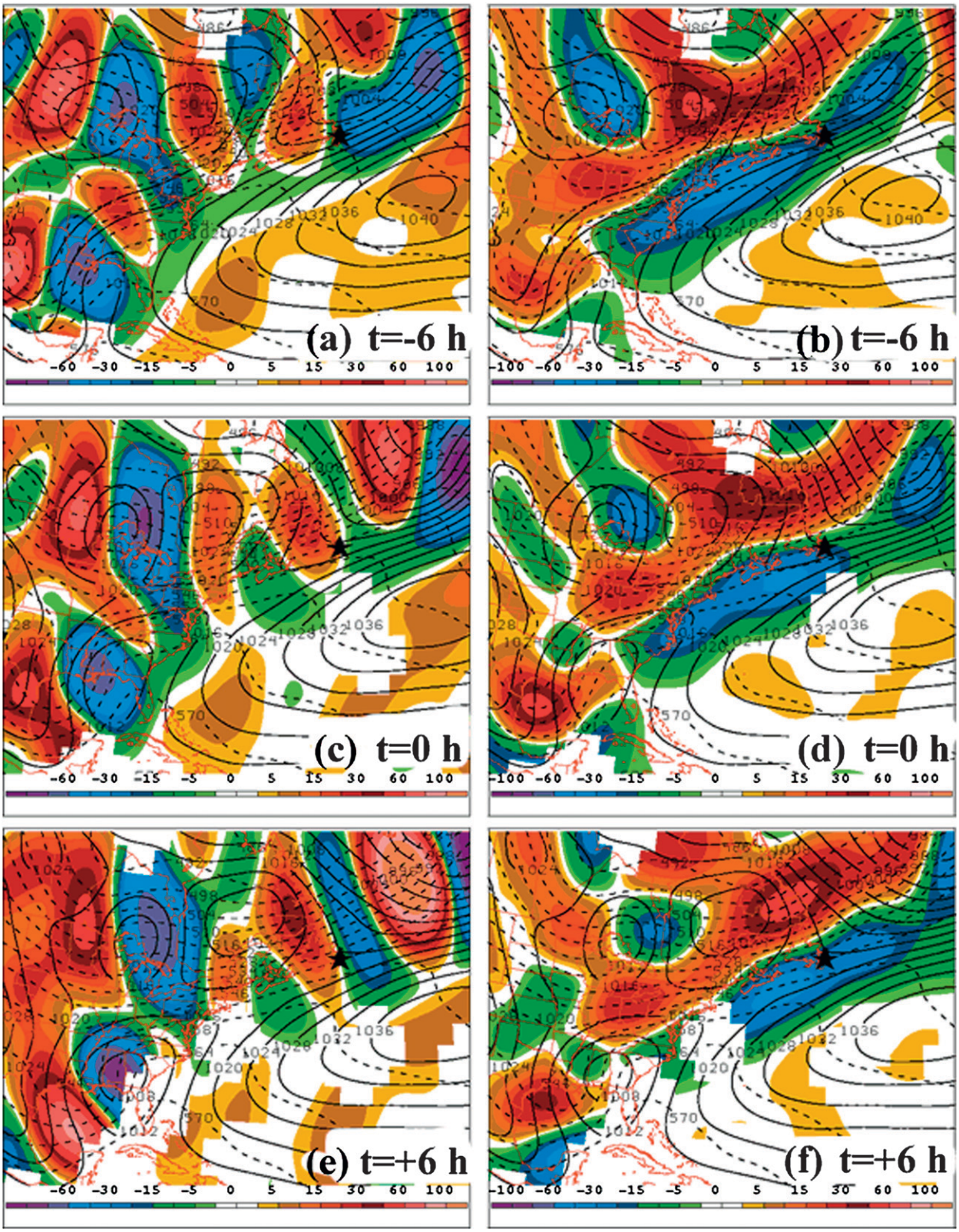

FIG. 17. For MAG 2, NCEP–NCAR Global Reanalysis plots of (left) 850–500-hPa layer-averaged $\mathbf{Q}_s$ and (right) $\mathbf{Q}_n$ divergence $\times 10^{-17}$ K m^{-2} s^{-1}, from t = (a),(b) −6, (c),(d) 0, and (e),(f) +6 h. Cool (warm) colors represent convergence (divergence).

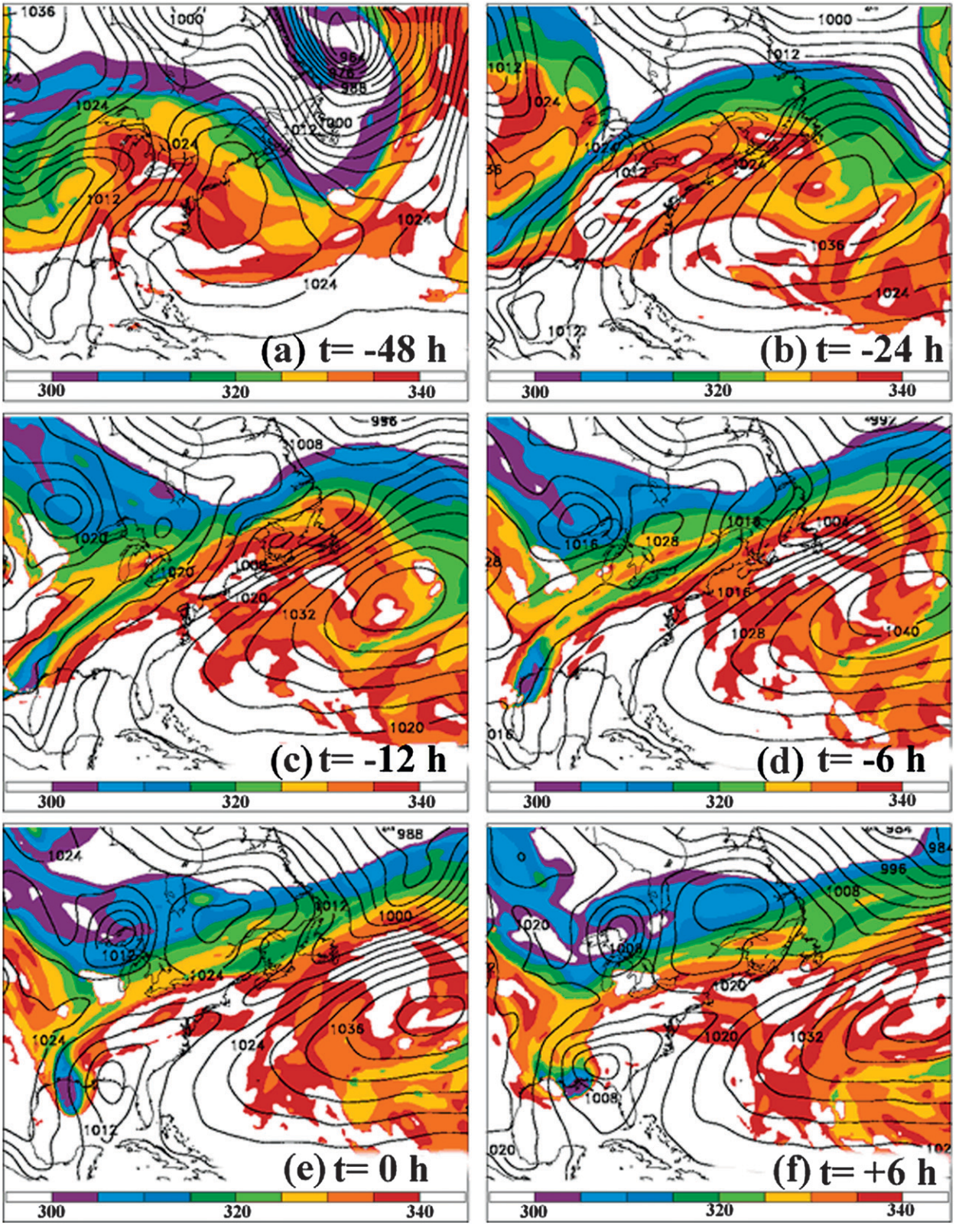

FIG. 18. Time series of GFS 1/2° analysis SLP (solid) contoured every 4 hPa, and potential temperature (K) on the dynamic tropopause (2-PVU surface, shaded), for MAG 2. Results are shown for t = (a) −48, (b) −24, (c) −12, (d) −6, (e) 0, and (f) t = +6 h, where t = 0 h is 0600 UTC 11 Dec 2008.

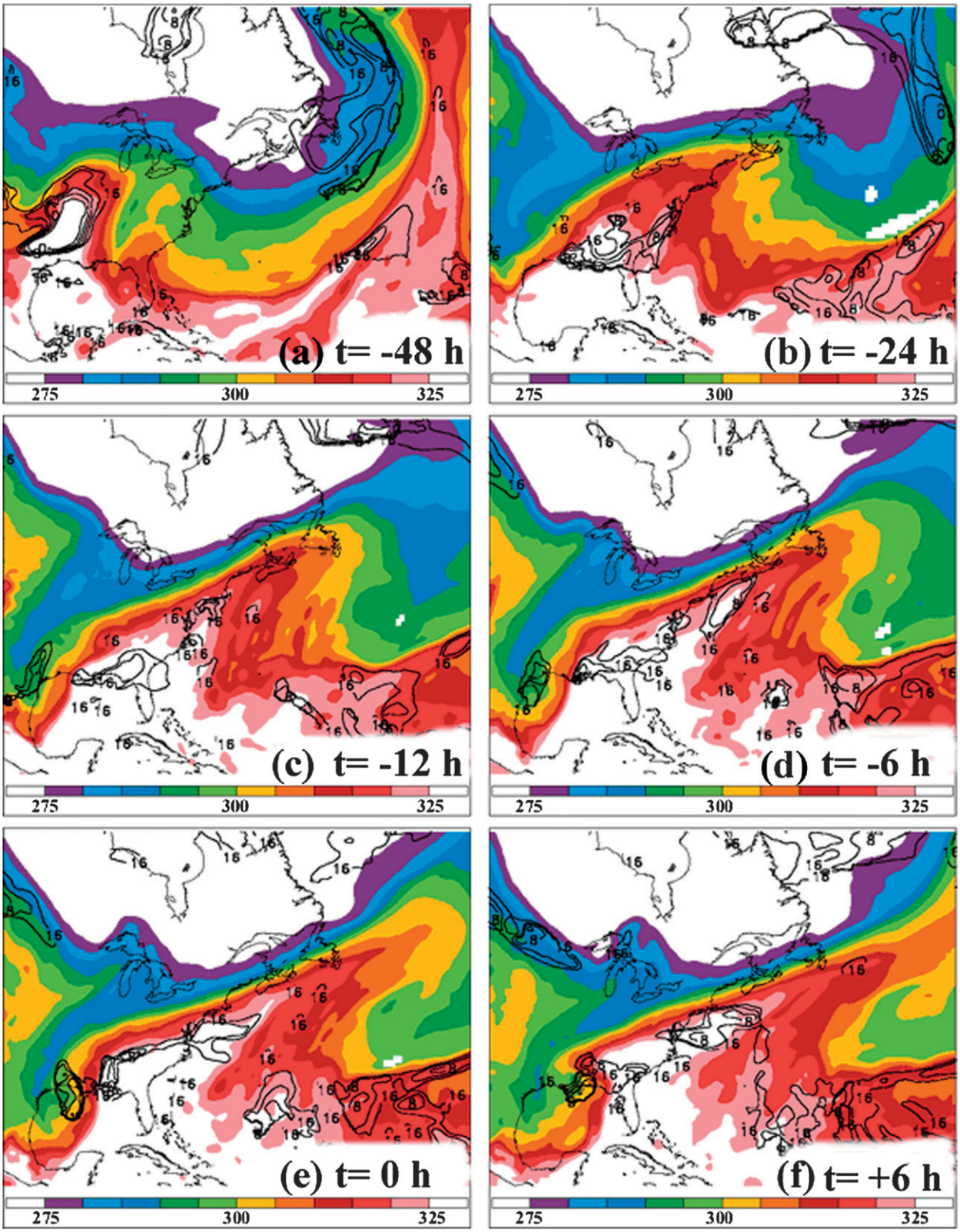

FIG. 19. As in Fig. 18, but for 850-hPa equivalent potential temperature (K, shaded), and CI (solid, every 4 K from 0 to +16).

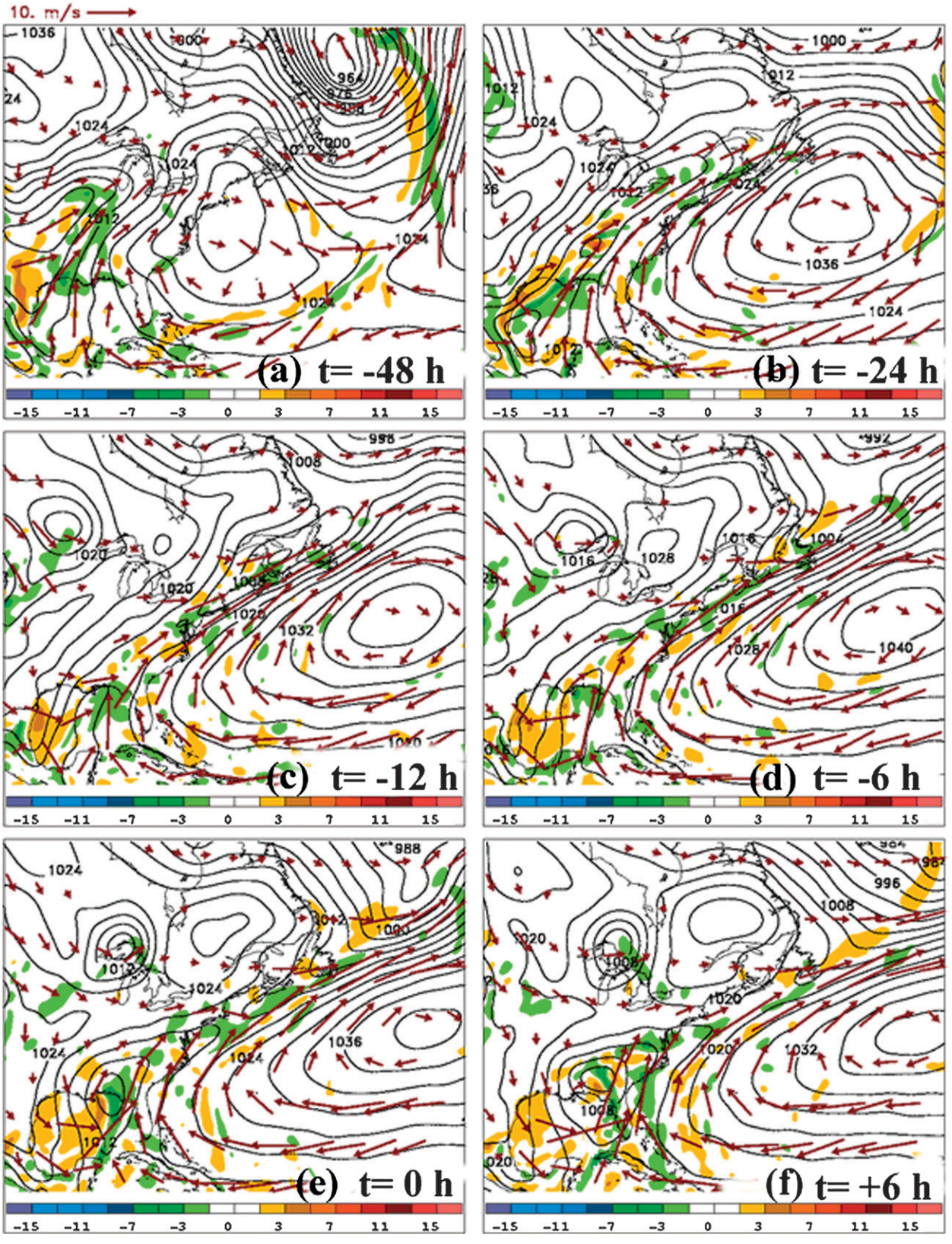

FIG. 20. As in Fig. 18, but for SLP (solid, every 4 hPa), 1000–700-hPa moisture flux convergence ($\times 10^{-8}$ kg m^{-2} s^{-1}, shaded), and 1000–700-hPa moisture transport vectors (g kg^{-1} m s^{-1}, red), with reference vector in the top left-hand corner.

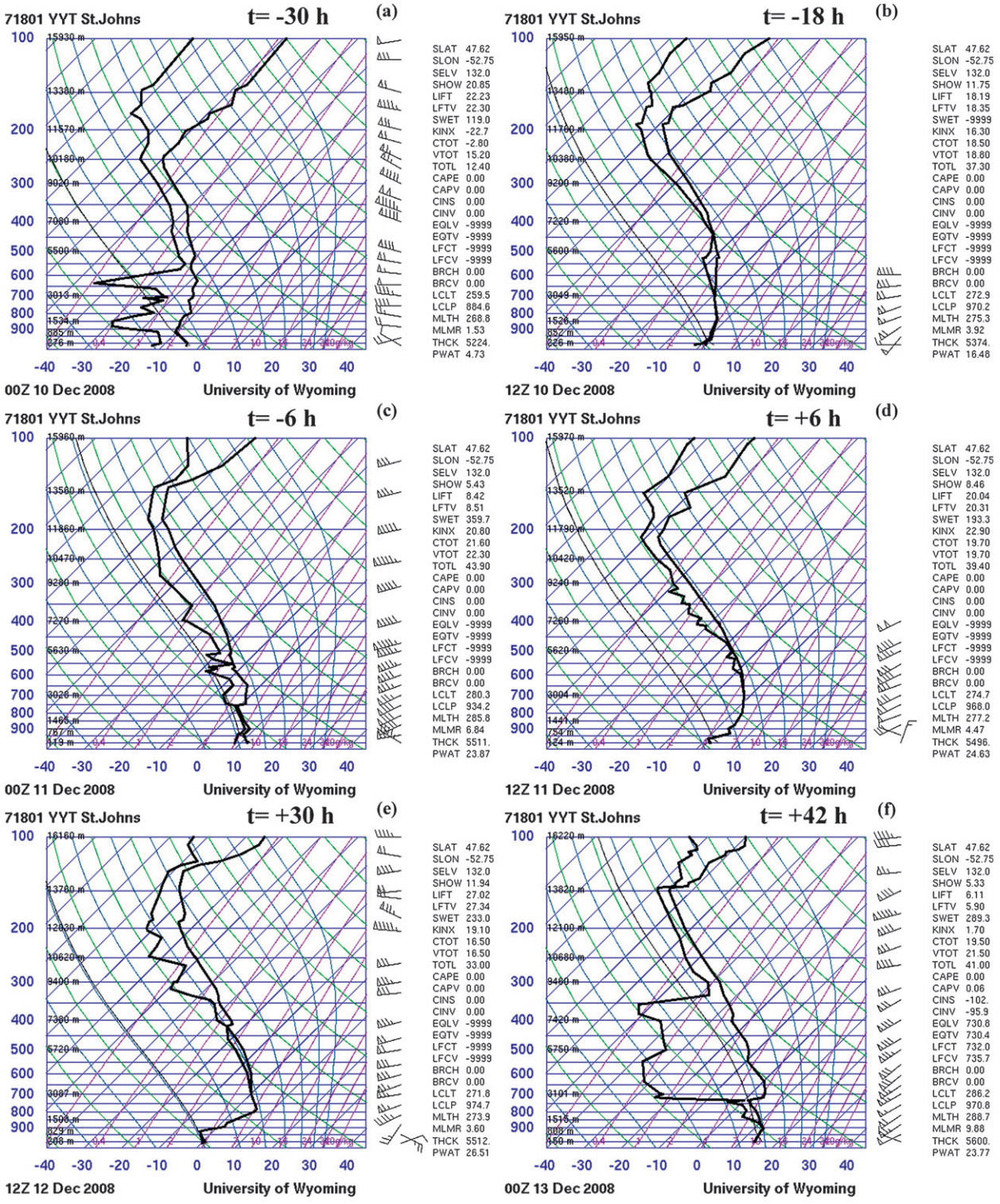

FIG. 21. Time series of observed soundings at CYYT for MAG 2. Soundings are shown for t = (a) −30, (b) −18, (c) −6, (d) +6, (e) +30, and (f) +42 h, where t = 0 h is 0600 UTC 11 Dec 2008. The sounding from t = +18 h is missing in the dataset.

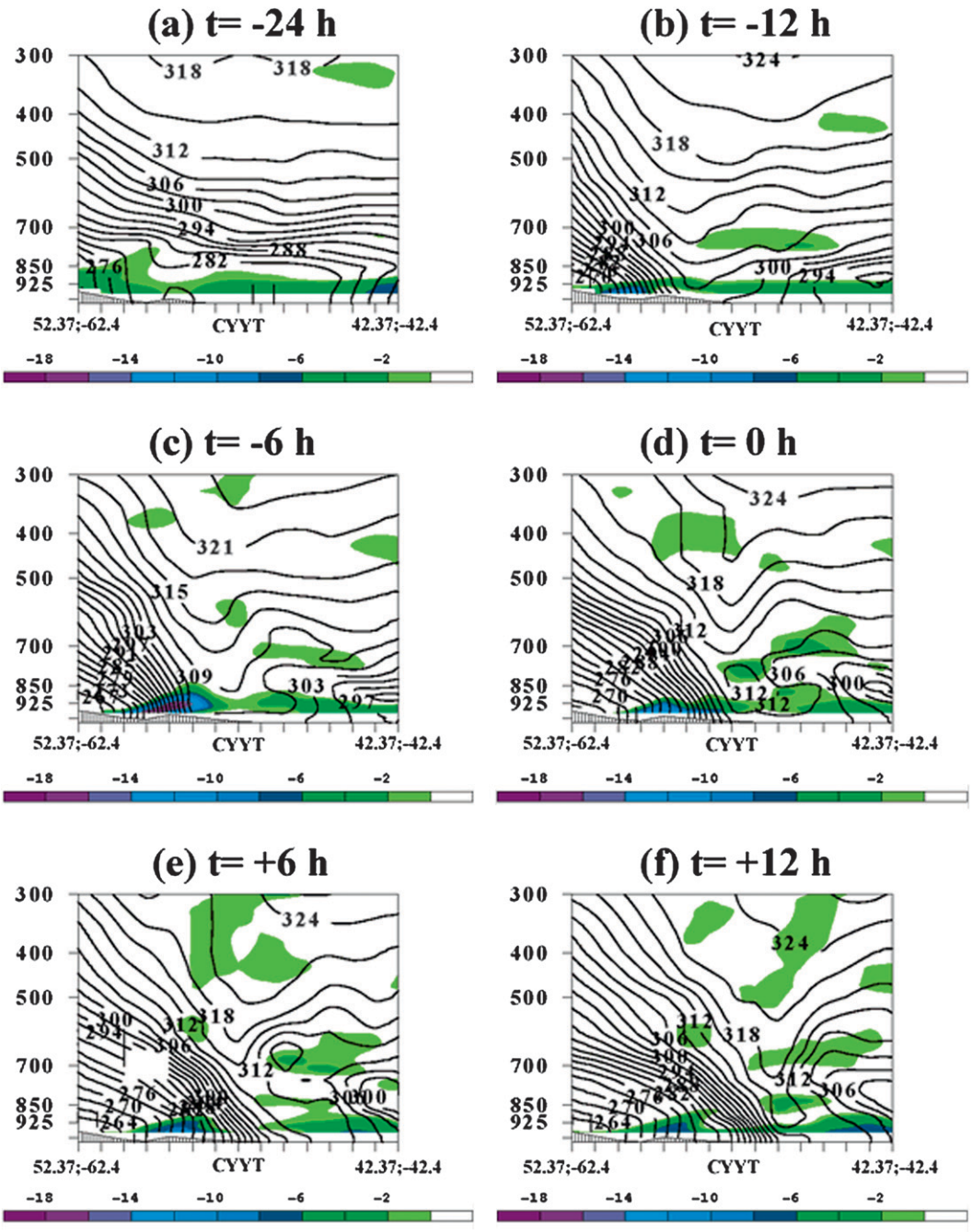

FIG. 22. Time series of northwest–southeast cross-section plots from 52.37°N, −62.4°W to 42.37°N, −42.4°W, for MAG 2. Saturated equivalent geostrophic potential vorticity ($\times 10^{-7}$ m^2 s^{-1} K kg^{-1}, shaded for negative values), equivalent potential temperature (K, contoured) shown for t = (a) −24, (b) −12, (c) −6, (d) 0, (e) +6, and (f) t = +12 h, where t = 0 h is 0600 UTC 11 Dec 2008. The location of CYYT is marked in each panel.

precipitation in MAG 2 fell during the cold frontal passage, the longevity and quasi-stationary nature of the baroclinic zone was important in the production of the remaining 30+ mm of precipitation. Additionally, observed soundings at CYYT during MAG 2 show that the tropopause remained exceedingly high for December for the duration of the event (Fig. 21).

It is reasonable to conclude that the approximately 20-mm difference in precipitation between MAG 1 and MAG 2 is related to the main points discussed in section 2b.

More specifically, while both events were characterized by the presence of a warm and moist subtropical air mass at CYYT, the overall values of Q-vector convergence and static stability in MAG 1 were substantially more conducive to a more extreme precipitation event. Nevertheless, the fact that MAG 2 exceeded the median extreme event at CYYT by 10 mm substantiates the importance of strong low-level frontogenesis over a long period of time (48 h) in the presence of an extremely moist subtropical air mass. While this is not a common occurrence [11 cases from 1979 to 2005, as seen in Milrad et al. (2010)], it shows that these conditions can occasionally produce an extreme cool-season precipitation event at CYYT.

In summary, the examinations of MAG 1 and MAG 2 show that two extreme precipitation events at CYYT can be produced by entirely disparate synoptic regimes. In the near future, the authors hope to use the detailed synoptic analyses of MAG 1 and MAG 2 in this paper as a basis for an examination of the performance of the operational forecasts (both numerical and human) during these events.

Acknowledgments. This research has been supported by grants from the Natural Sciences and Engineering Research Council of Canada and the Canadian Foundation for Climate and Atmospheric Sciences. The authors thank the two anonymous reviewers for their helpful comments. Thanks to the National Centers for Environmental Prediction (NCEP) and the National Climatic Data Center (NCDC) for providing access to the GFS analyses and NCEP–NCAR Global Reanalysis. We would also like to acknowledge the University of Wyoming's Department of Atmospheric Science Web site for providing access to the soundings in this manuscript. Finally, thanks to Gerard Morin at the Atlantic Climate Centre of Environment Canada for providing the 6-hourly precipitation data and the Holyrood radar imagery.

REFERENCES

Aguado, E., and J. E. Burt, 2007: *Understanding Weather and Climate*. Prentice Hall, 562 pp.

Bluestein, H., 1992: *Principles of Kinematics and Dynamics*. Vol. 1, *Synoptic–Dynamic Meteorology in Midlatitudes,* Oxford University Press, 431 pp.

Bosart, L. F., 1981: The Presidents' Day snowstorm of 18–19 February 1979: A subsynoptic-scale event. *Mon. Wea. Rev.,* **109,** 1542–1566.

——, and S. C. Lin, 1984: A diagnostic analysis of the Presidents' Day storm of February 1979. *Mon. Wea. Rev.,* **112,** 2148–2177.

——, and G. M. Lackmann, 1995: Postlandfall tropical cyclone intensification in a weakly baroclinic environment: A case study of Hurricane David (September 1979). *Mon. Wea. Rev.,* **123,** 3268–3291.

——, G. J. Hakim, K. R. Tyle, M. A. Bedrick, W. E. Bracken, M. J. Dickinson, and D. M. Schultz, 1996: Large-scale antecedent conditions associated with the 12–14 March 1993 cyclone (''Superstorm '93'') over eastern North America. *Mon. Wea. Rev.,* **124,** 1865–1891.

Brennan, M. J., and G. M. Lackmann, 2006: Observational diagnosis and model forecast evaluation of unforecasted incipient precipitation during the 24–25 January 2000 East Coast cyclone. *Mon. Wea. Rev.,* **134,** 2033–2052.

Dickinson, M. J., L. F. Bosart, W. E. Bracken, G. J. Hakim, D. M. Schultz, M. A. Bedrick, and K. R. Tyle, 1997: The March 1993 Superstorm cyclogenesis: Incipient phase synoptic- and convective-scale flow interaction and model performance. *Mon. Wea. Rev.,* **125,** 3041–3072.

Dirks, R. A., J. P. Kuettner, and J. A. Moore, 1988: Genesis of Atlantic Lows Experiment (GALE): An overview. *Bull. Amer. Meteor. Soc.,* **69,** 148–160.

Emanuel, K. A., 1983: On assessing local conditional symmetric instability from atmospheric soundings. *Mon. Wea. Rev.,* **111,** 2016–2033.

Galarneau, T. J., Jr., and L. F. Bosart, 2006: An examination of the long-lived MCV of 10–13 June 2003. Preprints, *Severe Local Storms Symp.,* Atlanta, GA, Amer. Meteor. Soc., P1.32. [Available online at http://ams.confex.com/ams/pdfpapers/103470.pdf.]

Gyakum, J. R., 1991: Meteorological precursors to the explosive intensification of the *QE II* storm. *Mon. Wea. Rev.,* **119,** 1105–1131.

——, 2008: The application of Fred Sanders' teaching to current research on extreme cold-season precipitation events in the Saint Lawrence River Valley region. *Synoptic–Dynamic Meteorology and Weather Analysis and Forecasting: A Tribute to Fred Sanders, Meteor. Monogr.,* No. 55, Amer. Meteor. Soc., 241–250.

——, and R. E. Stewart, 1996: A multiscale analysis of a case of slow growth/rapid cyclogenesis during CASP II. *Atmos.–Ocean,* **34,** 17–50.

——, and P. J. Roebber, 2001: The 1998 ice storm—Analysis of a planetary-scale event. *Mon. Wea. Rev.,* **129,** 2983–2997.

——, D. Zhang, J. Witte, K. Thomas, and W. Wintels, 1996: CASP II and the Canadian cyclones during the 1989–92 cold seasons. *Atmos.–Ocean,* **34,** 1–16.

Hart, R. E., and R. H. Grumm, 2001: Using normalized climatological anomalies to rank synoptic-scale events objectively. *Mon. Wea. Rev.,* **129,** 2426–2442.

Huo, Z., D. Zhang, J. Gyakum, and A. Staniforth, 1995: A diagnostic analysis of the Superstorm of March 1993. *Mon. Wea. Rev.,* **123,** 1740–1761.

——, ——, and ——, 1996: The life cyclone of the intense IOP-14 storms during CASP II. Part I: Analysis and simulations. *Atmos.–Ocean,* **34,** 51–80.

Kalnay, E., and Coauthors, 1996: The NCEP/NCAR 40-Year Reanalysis Project. *Bull. Amer. Meteor. Soc.,* **77,** 437–471.

Keyser, D., M. J. Reeder, and R. J. Reed, 1988: A generalization of Petterssen's frontogenesis function and its relation to the forcing of vertical motion. *Mon. Wea. Rev.,* **116,** 762–780.

Koch, S., M. DesJardins, and P. Kocin, 1983: An interactive Barnes objective map analysis scheme for use with satellite and conventional data. *J. Appl. Meteor.,* **22,** 1487–1503.

Kocin, P. J., P. N. Schumacher, R. F. Morales, and L. W. Uccellini, 1995: Overview of the 12–14 March 1993 Superstorm. *Bull. Amer. Meteor. Soc.,* **76,** 165–182.

Mekis, E., and W. D. Hogg, 1999: Rehabilitation and analysis of Canadian daily precipitation time series. *Atmos.–Ocean,* **37,** 53–85.

Mesinger, F., and Coauthors, 2006: North American Regional Reanalysis. *Bull. Amer. Meteor. Soc.,* **87,** 343–360.

Milrad, S. M., E. A. Atallah, and J. R. Gyakum, 2009: Synoptic-scale characteristics and precursors of cool-season precipitation events at St. John's, Newfoundland, 1979–2005. *Wea. Forecasting,* **24,** 667–689.

——, ——, and ——, 2010: Synoptic typing of extreme cool-season precipitation events at St. John's, Newfoundland, 1979–2005. *Wea. Forecasting,* **25,** 562–586.

Reuter, G. W., and M. K. Yau, 1990: Observations of slantwise convective instability in winter cyclones. *Mon. Wea. Rev.,* **118,** 447–458.

Roebber, P. J., and J. R. Gyakum, 2003: Orographic influences on the mesoscale structure of the 1998 ice storm. *Mon. Wea. Rev.,* **131,** 27–50.

Sanders, F., and J. R. Gyakum, 1980: Synoptic-dynamic climatology of the ''bomb.'' *Mon. Wea. Rev.,* **108,** 1589–1606.

Schultz, D. M., and P. N. Schumacher, 1999: The use and misuse of conditional symmetric instability. *Mon. Wea. Rev.,* **127,** 2709–2732.

Stewart, R. E., 1991: Canadian Atlantic Storms Program: Progress and plans of the meteorological component. *Bull. Amer. Meteor. Soc.,* **72,** 364–371.

——, and N. R. Donaldson, 1989: On the nature of rapidly deepening Canadian east coast winter storms. *Atmos.–Ocean,* **27,** 87–107.

——, R. W. Shaw, and G. A. Isaac, 1987: Canadian Atlantic Storms Program: The meteorological field project. *Bull. Amer. Meteor. Soc.,* **68,** 338–345.

——, C. A. Lin, and S. R. Macpherson, 1990: The structure of a winter storm producing heavy precipitation over Nova Scotia. *Mon. Wea. Rev.,* **118,** 411–426.

Uccellini, L. W., 1986: The possible influence of upstream upper-level baroclinic processes on the development of the *QE II* storm. *Mon. Wea. Rev.,* **114,** 1019–1027.

——, P. J. Kocin, R. A. Petersen, C. H. Wash, and K. F. Brill, 1984: The Presidents' Day cyclone of 18–19 February 1979: Synoptic overview and analysis of the subtropical jet streak influencing the pre-cyclogenetic period. *Mon. Wea. Rev.,* **112,** 31–55.

——, D. Keyser, K. F. Brill, and C. H. Wash, 1985: The Presidents' Day cyclone of 18–19 February 1979: Influence of upstream trough amplification and associated tropopause folding on rapid cyclogenesis. *Mon. Wea. Rev.,* **113,** 962–988.

Wash, C. H., S. M. Heikkinen, C. Liou, and W. A. Nuss, 1990: A rapid cyclogenesis event during GALE IOP 9. *Mon. Wea. Rev.,* **118,** 375–391.

Whitaker, J. S., L. W. Uccellini, and K. F. Brill, 1988: A model-based diagnostic study of the rapid development phase of the Presidents' Day cyclone. *Mon. Wea. Rev.,* **116,** 2337–2364.

Yau, M. K., and M. Jean, 1989: Synoptic aspects and physical processes in the rapidly intensifying cyclone of 6–8 March 1986. *Atmos.–Ocean,* **27,** 59–86.